Measurement of relative statetostate rate constants for the reaction D+H2(v, j)→HD(v',j')+H

David E. Adelman, Neil E. Shafer, Dahv A. V. Kliner, and Richard N. Zare

Citation: The Journal of Chemical Physics **97**, 7323 (1992); doi: 10.1063/1.463504
View online: http://dx.doi.org/10.1063/1.463504
View Table of Contents: http://scitation.aip.org/content/aip/journal/jcp/97/10?ver=pdfcov
Published by the AIP Publishing

Measurement of relative state-to-state rate constants for the reaction $D+H_2(v, j)\rightarrow HD(v', j')+H$

David E. Adelman, Neil E. Shafer, Dahv A. V. Kliner,[a] and Richard N. Zare
Department of Chemistry, Stanford University, Stanford, California 94305

(Received 5 June 1992; accepted 6 August 1992)

We have measured state-to-state integral rate constants for the reaction $D+H_2(v,j)\rightarrow HD(v'=0,1,2;j')+H$, in which the H_2 reagent was either in the ground state, $H_2(v=0,j)$, or prepared in the first excited vibrational state, $H_2(v=1, j=1)$, by stimulated Raman pumping. Translationally hot D atoms were produced via UV photolysis of DI, generating two center-of-mass collision energies corresponding to the two I atom spin–orbit states. Resonance-enhanced multiphoton ionization and time-of-flight mass spectrometry were employed to detect the nascent HD product in a quantum-state-specific manner. Two experimental geometries were used: (1) a probe-laser-induced geometry, in which the same laser both initiated the reaction, by photolysis of DI, and detected the HD and (2) an independent-photolysis-source geometry, in which photolysis of DI was carried out by an independent laser. We find that vibrational excitation of the H_2 reagent results in substantial HD rotational excitation for each product vibrational state, a shift in the vibrational product state distribution such that the rates for the reaction $D+H_2(v=1, j=1)$ into $HD(v'=0)$ and $HD(v'=1)$ are comparable, and somewhat surprisingly, almost no change in the total rate into $HD(v'=0,1,2;j')$. The experimental results are consistent with a model in which internal energy is conserved, i.e., internal energy of the reagents appears as internal energy of the products, while relative translational energy of the reagents appears primarily as translation of the products. Good to excellent agreement is found between the experiment and recent quantum-mechanical scattering calculations of Neuhauser, Judson, and Kouri. Minor discrepancies persist, however, between theory and experiment for some product rotational distributions.

I. INTRODUCTION

J. Polanyi's classic paper, Ref. 1, begins with "To the extent that chemistry can be regarded as existing separately from physics [the development by London, Eyring, and M. Polanyi of the first H_3 potential-energy surface in 1929] was a landmark in the history of chemistry, comparable in importance to the landmark in the history of physics marked by the appearance of the Heitler–London equation for H_2." Since the capacity for rigorous quantum-mechanical (QM) calculations was first realized, theoreticians have relied on the $H+H_2$ system as the starting point for a theoretical description of chemical reaction dynamics. Like the H_2 molecule in molecular spectroscopy, the relative simplicity of the $H+H_2$ reaction makes this system the benchmark for testing reactive scattering calculations. This simplicity arises from the limited number of particles, the large internal energy level spacings, and the fact that the reaction is restricted to a single adiabatic electronic surface for energies below $\sim$2.6 eV. During the latter half of the 1980's, parallel developments in theoretical and experimental techniques have resulted in unprecedented advances in the study of this system. These developments have allowed the $H+H_2$ reaction family to be investigated in remarkable detail and have provided the first direct comparisons between well-characterized experimental measurements[2–13] and fully converged, three-dimensional QM scattering calculations.[14–25]

In this paper we report new state-to-state rate constant measurements for the reaction $D+H_2(v=0,1;j)\rightarrow HD(v'=0,1,2;j')+H$. This system continues to challenge experimentalists and theorists alike because of outstanding discrepancies between measured and predicted results. Comparison is made with recent QM calculations of Neuhauser, Judson, and Kouri[26,27] (NJK) that accurately model the experimental conditions. The new measurements provide a detailed and global test of QM theory over a broad range of initial conditions. Good to quantitative agreement between QM theory and experiment is found; however, some differences remain that are outside of experimental uncertainty.

During the past four years, several direct comparisons between QM theory and experiment have been made for various isotopic variants of the $H+H_2$ reaction. Generally, excellent agreement has been found. Specifically, quantitative agreement exists between experiment and QM theory for (1) total reaction cross sections for the reactions $H+D_2(v=0)$ at $E_{rel}=1.3$ eV and $D+H_2(v=1)$ at $E_{rel}=0.33$ eV,[5,6,22] and (2) product-state-resolved, integral cross sections in which the molecular reagent was in the ground vibrational state for the reactions $H+$*para*-

[a]Present address: Department of Chemistry, University of Minnesota, Minneapolis, Minnesota 55455.

$H_2 \rightarrow H_2(v'=1,j')+H$ at $E_{rel}=0.83$–1.00 eV,[14,12] $H+D_2 \rightarrow HD(v'=1,j')+D$ at $E_{rel}=1.3$ and 0.55 eV,[2,7,22] and $D+H_2 \rightarrow HD(v'=1,j')+H$ at $E_{rel}=1.0$ eV,[18,28,21] where E_{rel} is the relative collision energy.

Despite this general agreement, some outstanding discrepancies remain for differential cross sections of the $D+H_2$ reaction and for integral rate constants of the reaction $D+H_2(v=1, j=1) \rightarrow HD(v'=1,j')+H$. Two groups have performed differential cross section measurements for the $D+H_2$ reaction. Buntin, Giese, and Gentry[4,8] carried out experiments at a fixed laboratory scattering angle with variable E_{rel}, whereas the study of Continetti, Balko, and Lee[10] included numerous scattering angles for two values of E_{rel}, 1.01 and 0.53 eV. Quantitative disagreements were found between each of these studies and Monte Carlo simulations of the experiments using the QM calculations of Zhang and Miller[18] and of Zhao *et al.*[21] These discrepancies were tentatively attributed to inaccuracies in the H_3 bend potential.[10] A recent reevaluation of the H_3 bend potential by Bauschlicher, Langhoff, and Partridge,[29] however, found only very minor deviations between the double many-body expansion (DMBE) surface[30] and the new *ab initio* points; in particular, the DMBE surface agrees with all of the *ab initio* points to within 1.13 kcal/mol. Integral cross-section measurements of the reaction $D+H_2(v=1, j=1) \rightarrow HD(v'=1,j')+H$ at $E_{rel}=1.0$ eV by Kliner, Adelman, and Zare[13] (KAZ) were in qualitative agreement with the QM calculation of Blais *et al.*,[19] but quantitative discrepancies were also found.

Initial work on the reaction $D+H_2(v=1, j=1) \rightarrow HD(v'=1,j')+H$ at $E_{rel}=1.0$ eV was reported by Kliner and Zare (KZ).[9] These measurements were followed by a more complete study by KAZ. The H_2 reagent was prepared in the level $(v=1, j=1)$ via stimulated Raman pumping (SRP), and (2+1) resonance-enhanced multiphoton ionization (REMPI) was utilized for quantum-state-specific detection of the nascent HD product.[31] In these experiments the probe laser both initiated the reaction by photolysis of DX (X=Br or I) and state specifically ionized the HD product, all within the ~5 ns pulse duration; consequently, E_{rel} varied with HD rovibrational level detected. Photolysis of DBr (DI) gives E_{rel} values of approximately 1.0 and 0.8 eV (1.4 and 0.9 eV), where the two collision energies correspond to concurrent production of ground-state $X(^2P_{3/2}) \equiv X$ and spin–orbit excited $X(^2P_{1/2}) \equiv X^*$. Both studies used essentially the same experimental setup with the exception of two improvements in the later experiment: First, the use of a higher-power injection-seeded Nd:YAG laser almost tripled the fraction of the H_2 reagent population pumped into $(v=1, j=1)$. Second, the collision-energy spread was reduced by a factor of 5 to ~0.07 eV full width at half maximum (FWHM) by changing the reagent-beam source from a continuous, effusive nozzle to a pulsed, supersonic nozzle.

KAZ included several experimental checks; among the most important of these were (1) the determination that for the range of reagent j states populated, integral rate constants for the reaction $D+H_2(v=0,j)$ do not depend, in an observable manner on j, and (2) the use of two photolytic D-atom sources (DBr and DI). There was good agreement between the results of KZ and KAZ for the experiment using DBr as the photolytic precursor and the results of the experiment using photolysis of DI were consistent with the DBr work. This second result should be emphasized because the most significant source of noise for the DBr experiment was the production of D^+ ions, a problem largely absent from the experiment using DI. Thus, the consistency between the DI and DBr results suggested to KAZ that interference by D^+ was not systematically perturbing the DBr distribution. KAZ concluded that the discrepancy with the QM calculation of Blais *et al.* persisted. In particular, the predicted rotational distribution was too hot by 2–3 quanta. In addition, the calculated ratio of the rates into $v'=1$ for the reaction with $H_2(v=1, j=1)$ versus H_2 (thermal) was too large by 67%. Later computational checks and more rigorous calculations found minor errors, at most 10%, in the QM calculations.[19,25] These improvements did not bring theory and experiment into closer agreement.

In this paper we report new measurements for the reaction $D+H_2(v,j) \rightarrow HD(v'=0,1,2;j')+H$ at $E_{rel}=1.4$ and 0.9 eV and at $E_{rel}=0.8$ eV. Measurement of the rates into $v'=0$ and 2 were recorded using the experimental arrangement described previously, in which the probe laser both initiated the reaction via DI photolysis and detected the HD product via REMPI. In other experiments, an independent photolysis source was introduced because of the need for additional experimental checks and for measurements at lower values of E_{rel}. Specifically, an independent UV laser pulse was added to initiate the reaction by photolysis of DI, thereby decoupling the photolysis and probe steps. This experimental arrangement offers more flexibility in selecting the initial conditions by providing independent control of the reagent rovibrational state, E_{rel}, and the product rovibrational state probed. The thermal energy spread remained ~0.07 eV FWHM, but the variation in E_{rel} with j' was eliminated by having a fixed-wavelength photolysis source. Considerable time was spent testing for possible sources of systematic error associated with the constrained reaction volume imposed by using focused laser beams. We were particularly concerned about product fly out from the detection region. In addition, tests were performed to assess the reliability of DBr as a photolytic D-atom source.

During the course of this study, NJK completed a new set of QM calculations for the $D+H_2$ reaction.[26] These calculations were performed over a range of collision energies wide enough that a *complete simulation* of the experimental initial conditions could be carried out, as was done for the $H+para\text{-}H_2$ study[12] but not for the previous $D+H_2$ work.[9,13] This simulation takes into account the variation in E_{rel} with rovibrational state probed for the probe-laser-induced reaction, the experimental collision energy spread, and the fast and slow D-atom contributions associated with the production of X/X^* in the photolysis of DX, including the variation in the X/X^* ratio with j' for the probe-laser-induced reaction. Excellent agreement is

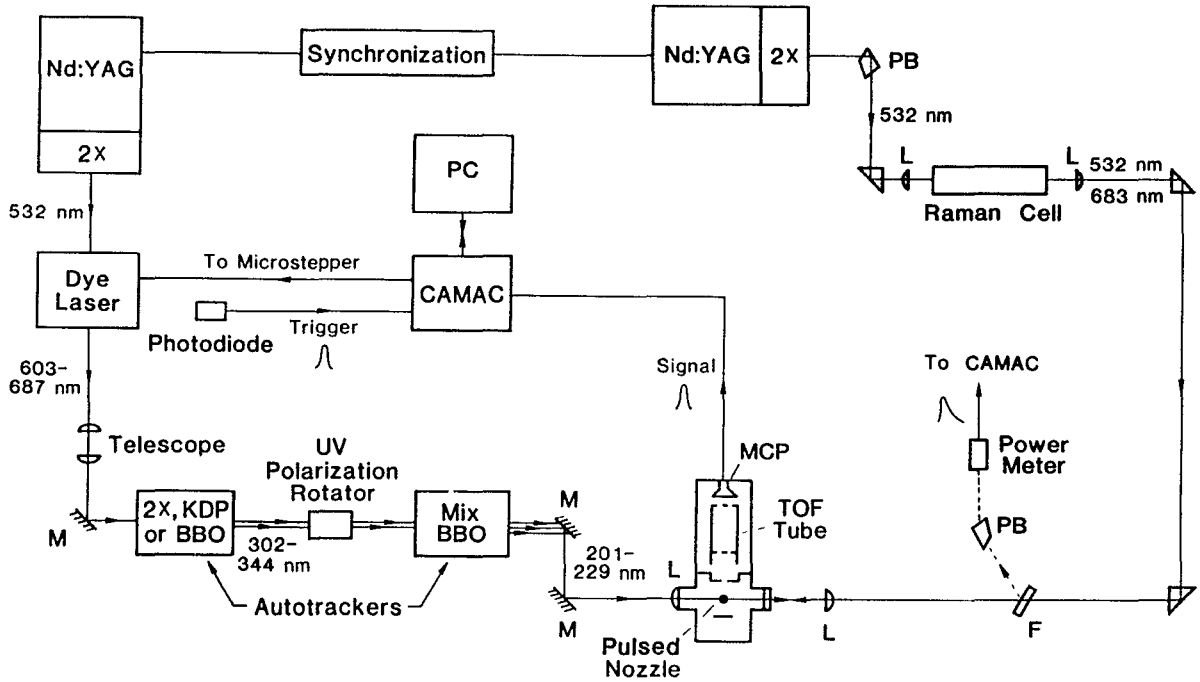

FIG. 1. Schematic diagram of the probe-laser-photolysis (PLP) experimental geometry. *M* is the dichroic mirror, *L* the lens, PB the Pellin Broca prism, *F* the BK-7 flat, MCP the multichannel plate detector, and PC the personal computer.

found between the predicted and measured values for the vibrational branching ratios and the enhancement in the rate into a specific v' level upon vibrational excitation of the H_2 reagent. Nevertheless, small differences persist outside of experimental uncertainty between the measured and predicted product rotational distributions. These differences are most pronounced at the highest energies and for those distributions in which a large fraction of the energy appears in the translational degree of freedom of the reaction products.

II. EXPERIMENT

This section has five subsections. In Sec. II A, two experimental arrangements are described. In the first arrangement, which we refer to as the "probe-laser-photolysis" (PLP) geometry, the probe laser both initiated the reaction via photolysis of DX and detected the HD product via REMPI. In the second arrangement, which we refer to as the "independent-laser-photolysis" (ILP) geometry, an independent laser pulse was used as the photolysis source. These two setups share many common features and, consequently, are presented together. In Sec. II B, we describe experimental checks carried out to test for interfering reactions, the probe-laser power dependence, product fly-out, and the dependence of the ILP rotational distributions on the time delay between the photolysis and probe lasers. The results of the first three tests demonstrated that systematic errors were not contributing to the measurements outside of experimental uncertainty. For the last test, a systematic bias was found that could be accounted for in our analysis of the data. We include in Sec. II C a brief description of tests carried out on the reaction $D+H_2(v=1,j=1)\rightarrow HD(v'=1,j')+H$ using the DBr photolytic precursor. In Sec. II D, we present the experimental procedure and, in Sec. II E, the calibration of the REMPI detection scheme.

A. Experimental designs

1. Apparatus

Overviews of the PLP and the ILP experimental setups are shown in Figs. 1 and 2, respectively. The vacuum chamber is detailed in Fig. 3. DX (X=Br or I, Cambridge Isotope Labs, 99% D stated isotopic abundance) was purified by a freeze–pump–thaw cycle and mixed with H_2 (Linde, 99.9995+% stated purity) and He (Linde, 99.9995% stated purity) in the ratio DX:H_2:He=1:3–4:15–30. The reagent mix flowed into a high-vacuum chamber via a pulsed, supersonic nozzle. The measured rotational temperature of H_2 was 150 K for these experiments.[13] This vertical reagent beam was crossed by the focused, copropagating SRP beams ($\lambda=532$ and 683 nm). The SRP beams were focused into the chamber by a quartz lens (200 mm f.l.) mounted on an *x-y-z* translation stage, thereby allowing optimization of their overlap with the counterpropagating probe beam, which was also focused by a quartz lens (125 mm f.l.). For the PLP system the probe/photolysis laser ($\lambda\approx210$ nm) was fired 15–20 ns after the SRP pulses to photodissociate DX, yielding fast D atoms. This laser pulse also state-specifically ionized the HD reaction product via (2+1) REMPI. Because the same laser pulse effected both photolysis and detection, the observed reaction products were formed within the ~5 ns pulse duration. The HD^+ ions were detected in a shuttered time-of-flight mass spectrometer (TOF-MS).[32]

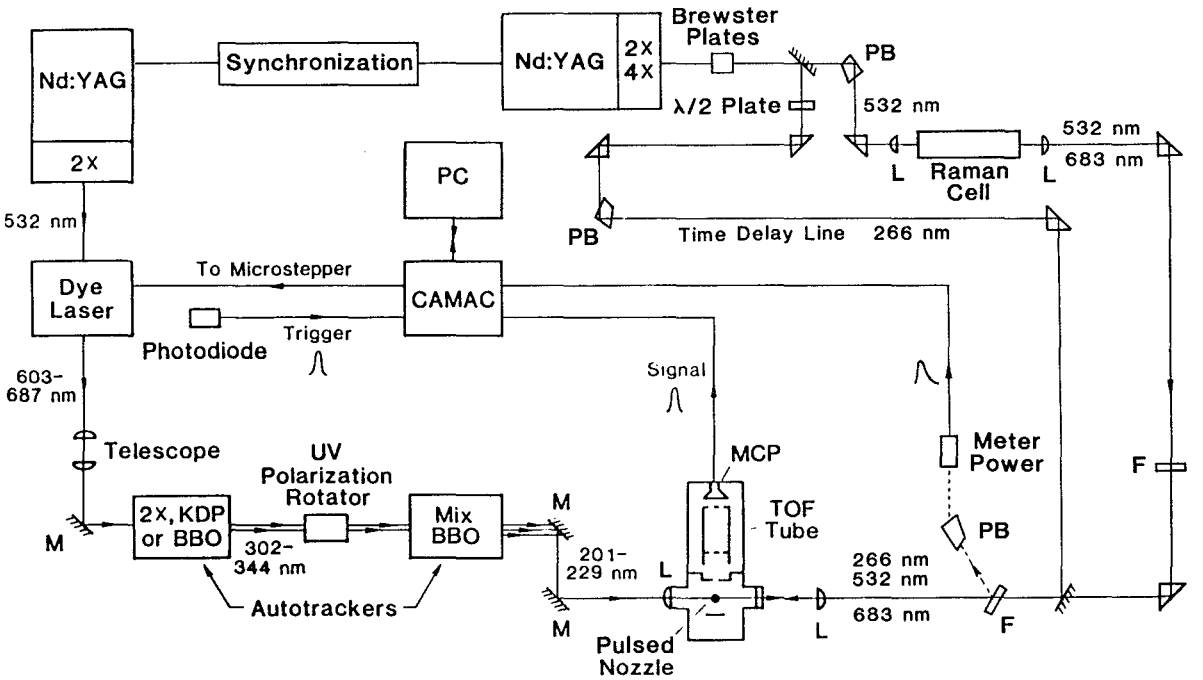

FIG. 2. Schematic diagram of the independent-laser-photolysis (ILP) experimental geometry. *M* is the dichroic mirror, *L* the lens, PB the Pellin Broca prism, *F* the Suprasil or BK-7 flat, MCP the multichannel plate detector, and PC the personal computer.

For the ILP arrangement, the copropagating photolysis pulse ($\lambda=266$ nm) was optically delayed by 15 ns with respect to the SRP beams. The photolysis beam was focused by the same lens as the SRP beams. Use of a telescope in the path of the photolysis beam allowed the position of its focus to be independently varied. In addition, adjustment of the angle of the dichroic mirror used to combine the photolysis and SRP beams permitted independent control of the overlap of the photolysis and probe-laser beams (Fig. 2). The probe-laser pulse followed the photolysis pulse after an electronically controlled delay of ~20 ns. For the $D+H_2(v=1, j=1)\rightarrow HD(v'=0,j')+H$ rotational product state distribution at $E_{rel}=1.35$ eV we used the same geometry as that described in Ref. 7. The fifth harmonic of a Nd:YAG laser was used to generate the 212.8 nm photolysis light.

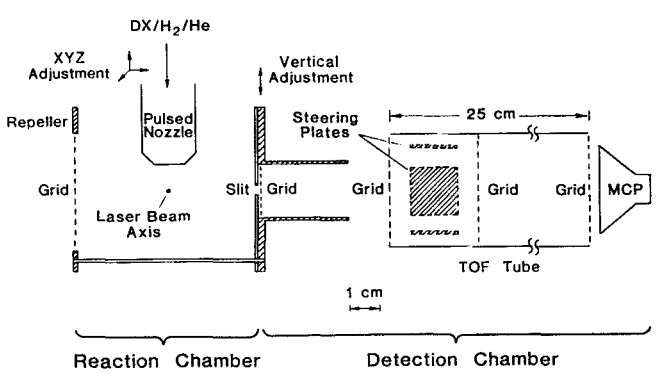

FIG. 3. Expanded view of the reaction and detection chambers.

As in previous ILP studies,[7,12] an every-other-shot subtraction procedure was used to remove the probe-laser-photolysis contribution to the ion signal. This procedure involved varying the delay between the photolysis and probe lasers between ~7 and ~20 ns on alternate pulses; see Fig. 4. At each delay the probe-laser-photolysis signal was the same; however, the independent-laser-photolysis reaction signal increased because of product buildup. Thus, subtraction of the ion signal at a 7 ns delay from that at a 20 ns delay provided signal exclusively from the independent-laser-photolysis reaction.

The probe laser consisted of a 10 Hz Nd:YAG pumped dye laser (Spectra-Physics, DCR-3G, PDL-1) with frequency doubling and mixing stages [INRAD Autotracker II, β-barium borate (BBO) crystals[33]]. A 10 Hz, injection-seeded Nd:YAG laser (Spectra-Physics, GCR-4) and H_2 filled Raman cell (pressure=29 psig) generated the SRP beams (Figs. 1 and 2). For the ILP geometry, the SRP Nd:YAG laser was used to generate both the SRP beams and the 266 nm photolysis beam (Fig. 2).

For the ILP geometry, the photolysis beam spot size had to be equal to or smaller than the SRP beams. If the photolysis beam were larger than the SRP beams, the effective $H_2(v=1, j=1)$ population would be diluted because D atoms generated outside of the SRP beam volume would react almost exclusively with ground-state H_2. An approximate measurement of the beam diameters of the SRP and photolysis beams was made using a knife-edge technique.[34] For these experiments the FWHM laser-beam diameters were 110 ± 12 and 83 ± 12 μm for the SRP and photolysis beams, respectively, assuming that the beam profiles were Gaussian.

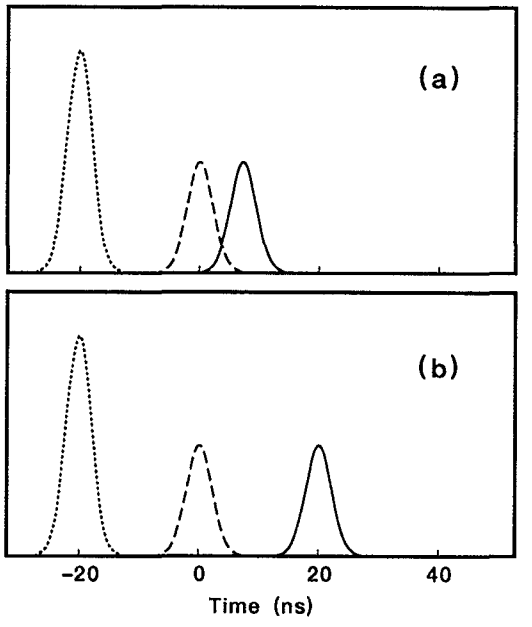

FIG. 4. Timing diagram for every-other-shot data collection. 20 ns before the photolysis laser was fired, the SRP pulses (dotted lines) prepared the H_2 reagent in the ($v=1, j=1$) level. At time $t=0$ the photolysis laser was fired (dashed lines). The reaction rate was extracted by subtracting the REMPI signal obtained from firing the probe laser 7 ns after the photolysis laser [solid line in (a)] from the REMPI signal obtained from firing the probe laser 20 ns after the photolysis laser [solid line in (b)].

2. Stimulated Raman pumping

The SRP setup was the same as previously described.[9,13] SRP allows the preparation of a single rovibrational level in the ground electronic state of a molecule. This technique requires two laser beams with a frequency difference that matches the Raman-allowed transition $H_2(v=0, j=1) \rightarrow H_2(v=1, j=1)$. The wavelengths of the SRP beams were 532 nm (second harmonic of the Nd:YAG laser) and 683 nm (first Stokes from the 532 nm beam passing through the Raman cell); see Figs. 1 and 2. The bandwidth of the 532 nm beam was ~ 0.007 cm^{-1} and that of the 683 nm beam was ~ 0.2 cm^{-1}.[35] The bandwidth of the 683 nm beam was much larger than the Doppler width of the $H_2(v=0,j) \rightarrow H_2(v=1, j=1)$ transition (~ 0.04 cm^{-1}), ensuring that the SRP efficiency was not affected by thermal motion of the H_2 molecules. The output of the Raman cell was passed through a BK-7 flat to remove the UV anti-Stokes orders that could photolyze DX. For the PLP geometry this flat also provided a back reflection of the counterpropagating ~ 210 nm photolysis/probe beam used for power normalization.

The SRP efficiency is defined as

$$1-[H_2(v=0,j=1) \text{ with SRP}]/[H_2(v=0,j=1) \text{ without SRP}], \quad (1)$$

where $[\cdots]$ denotes density. The SRP efficiency was measured by recording $H_2(v=0, j=1)$ REMPI spectra both with and without Raman pumping. The reduction in the area under the peak in the presence of the SRP beams equals the fraction of the population excited into ($v=1$, $j=1$). As in the previous experiment, a Raman pumping efficiency of 50% (saturation) corresponds to promotion of 35.5% of the thermal (150 K) H_2 into ($v=1, j=1$).

3. DX Photolysis

UV laser photolysis of DX (X=Br or I) was used to generate translationally hot D atoms. Photolysis of DX results in the production of two groups of D atoms with different speeds, which correspond to the production of X and X*. In the ILP experiment approximately 74% of the D atoms were produced via the fast channel,[36] where E_{rel} was 0.78 and 0.33 eV for the fast and slow D atom channels, respectively. QM calculations predict, however, that the slow D atoms do not react.[18]

In the PLP experiment, D atoms from the slow channel contribute to reaction. When DX was photolyzed by the tunable probe laser ($\lambda=202$–221 nm), the photolysis wavelength and, therefore, E_{rel} varied as different $HD(v',j')$ levels were detected. The variation in E_{rel} for DI photolysis over all rovibrational states measured (i.e., $HD(v'=0, j'=3)$ to $HD(v'=2, j'=11)$) was 1.51 to 1.30 eV for the fast channel and 1.04 to 0.79 eV for the slow channel. Within a given vibrational level E_{rel} changed by 0.16 eV for $HD(v'=0)$ and 0.06 eV for $HD(v'=2)$ using DI photolysis. The I*/I ratio varies with photolysis wavelength.[36] The faster D atoms had a higher collision frequency, which increased their contribution to the measured rates (Sec. II A 1). Therefore, the contribution of the slow D-atom channel to the measured distributions for $HD(v'=0,j')$ and $HD(v'=2,j')$ varied between 13–29% and 37–43%, respectively.

For DBr photolysis, the variation over $HD(v'=0, j'=4$–$12)$ was 1.15–1.07 eV for the fast channel and 0.94–0.87 eV for the slow channel. For DBr photolysis, the contribution of the Br* channel to the rate is expected to be approximately 13.5% and is essentially independent of photolysis wavelength.[37–39]

For the purposes of clarity we identify the E_{rel} of a reaction by simply referring to the value of E_{rel} for the fast D-atom channel. It should be recognized that both the fast and slow channels contributed, in general, to the measured product state distributions (and are included in theoretical simulations[26]), although the fast channel was dominant.

B. Experimental checks

1. SRP checks

Because of chromatic aberration, the position along the beam of the probe-laser focus varied by ~ 2 mm within each vibrational level and by ~ 5 mm for all rovibrational states measured.[40] This variation is significantly smaller than the calculated confocal parameters of ~ 1 cm for the probe laser and ~ 2 cm for the SRP beams.[40] The SRP efficiency was determined experimentally to be insensitive to changes of up to ~ 6 mm in the relative positions of the foci of the SRP and probe beams.

REMPI was used to verify that SRP did not populate rovibrational levels of H_2 other than $H_2(v=1, j=1)$. We

specifically confirmed that $H_2(v=1, j=0,2\text{–}4)$ and $H_2(v=0, j=3,4,7,12)$ were not populated by the presence of the SRP beams.

2. H(D)+DX(HX) *contamination*

The DX reagents both contained HX impurities. This isotopic impurity resulted in a small $HD(v',j')$ signal from the reactions H+DX and D+HX, which interfered with the $D+H_2$ reaction measurements. This small interference could be quantified by preparing the appropriate mix of He and DX and recording the $HD(v',j')$ signal. The HD signal from the $D+H_2$ reaction is linear in ["DX"], whereas those from D+HX and H+DX depend quadratically on ["DX"], where "DX" denotes DX containing HX impurity. To suppress these interfering reactions, the "DX" was made very dilute (3–4 %) in the reagent mix used for the $D+H_2$ studies. For the $HD(v'=0,j')$ rotational distributions using either DI or DBr, the "DX" was sufficiently dilute that the contributions of the D+HX and H+DX reactions to the total $HD(v'=0,j')$ signal were at most 5% of the smallest peak measured.

The $HD(v'=2,j')$ signal from the D(H)+HI(DI) reactions was less than 5% for $j'<9$ but could not be neglected for $j'\geqslant 9$. The $HD(v'=2$, high $j')$ signal from D(H)+HI(DI) was particularly problematic because these reactions produce highly rotationally and vibrationally excited HD product.[41–43] For $HD(v'=2, j'=9,10,11)$, spectral peaks were recorded with and without Raman pumping, allowing the D(H)+HI(DI) contributions to be subtracted directly. This subtraction procedure is valid because $j'=9$ has a negligible contribution from the $D+H_2(v=0)$ reaction and $j'=10$ and 11 are energetically inaccessible to this reaction. The subtracted contribution of the interfering reactions to the total signal was 7%, 11%, and 26% for $j'=9$, 10, and 11, respectively. For $HD(v'=2, j'=8)$, we estimate that the D(H)+HI(DI) contributions to the total population were less than 12% for the unpumped distribution and less than 2% for the pumped distribution. No attempt was made to subtract these minor contributions.

A direct subtraction of the D(H)+HI(DI) contribution was not carried out for the reaction $D+H_2(v=1, j=1)\rightarrow HD(v'=1,j')+H$ using the ILP setup ($E_{rel}=0.8$ eV). An approximate measurement of the contribution from the interfering reactions was made by assuming that the relative population measured for $j'=12$ arises entirely from the D(H)+HI(DI) reactions; thus, the measured population in $j'=12$ was set to zero. For $j'<9$ there was less than a 5% contribution from these reactions; for $j'=9$, 10, and 11 the contributions were 4%, 8%, and 24%, respectively. These contributions were subtracted. This procedure slightly overestimates the contribution from the competing reactions, although measurements of the D(H)+HI(DI) reactions suggested that this estimate was reasonably accurate.

No experimental estimate could be made for the contribution from the D(H)+HI(DI) reactions to the $D+H_2(v=0,j)$ reaction measurements. Because the $D+H_2(v=0,j)$ reaction produces a cold $HD(v'=1)$ rotational distribution [Fig. 12(a)], we expect that the contribution from the interfering reactions was minimal, except possibly for the highest j' states (i.e., $j'=6$ and 7), in which the signal levels were extremely low. No subtraction of these small interferences was made.

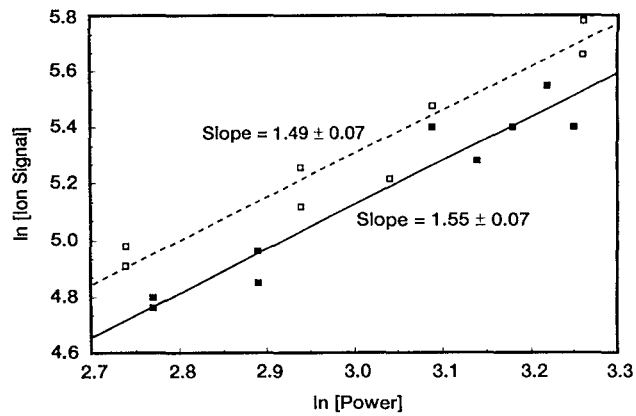

FIG. 5. Log–log plot of the REMPI signal intensity vs probe-laser pulse energy for the reaction $D+H_2(v=0,j)\rightarrow HD(v',j')+H$ at $E_{rel}=1.0$ eV. The data for $HD(v'=0, j'=11)$ (dashed line) have been arbitrarily offset from those for $HD(v'=1, j'=4)$ (solid line). Each point represents the average of two scans over the spectral peak. The lines indicate linear least-squares fits to the points.

3. Power dependence

In the (2+1) REMPI detection scheme the bound-free ionization step was saturated and the two-photon bound–bound transition was partially saturated. Consequently, we must consider how the ion signal depends on laser power so that we can extract relative populations. For the $HD(v'=0$ and 2) product rotational distributions, the power of the probe laser varied by ±25% across the vibrational band. In previous studies of the PLP $D+H_2$ reaction, only $HD(v'=1,j')$ product states were measured, for which the probe-laser power was constant. In the most recent $D+H_2(v=1, j=1)$ study[13] a power-dependence measurement was reported; however, this test involved a limited number of measurements and did not require an absolute value for the power dependence.

We report here a more systematic study, necessitated by the measurement of rates into $HD(v'=0$ and 2). Two Glan–Taylor polarizers were used to attenuate the probe-laser power, allowing the power to be reduced without changing the polarization, beam profile, divergence, or beam path. The power was varied by up to a factor of 2. A log–log plot of the integrated ion signal versus the probe-laser pulse energy for $HD(v'=0, j'=11)$ and $HD(v'=1, j'=4)$ is presented in Fig. 5; a linear least-squares fit to the data gives the laser power dependence of the REMPI signal, where the population is proportional to the ion signal divided by (laser power)^n. The power dependence, n, was determined to be 1.5 ± 0.3 for $HD(v'=0, j'=11)$ and 1.5 ± 0.2 for $HD(v'=1, j'=4)$. These values are comparable to previous measurements of 1.4 ± 0.2.[31] The power correc-

tion of 1.4 was therefore used in extracting populations from the measured ion signals.

4. Product fly-out

To convert the measured ion signals to relative populations, we had to ensure that the detection procedure did not discriminate against any product states because of "product fly-out." Two possible mechanisms could contribute to product fly-out: (1) Fly-out from the detection volume, in which HD molecules escape the detection volume before being ionized and (2) HD^+ ion extraction loss, in which HD^+ ions do not pass through the extraction slit (Fig. 3). The following tests demonstrated that product fly-out was not significant for the present measurements.

The $D+H_2$ reaction is more susceptible to systematic errors caused by product fly-out than are the other isotopic variants. For this isotopic combination and these values of E_{rel}, the laboratory velocity of the center of mass of the system and the HD velocity in the center-of-mass frame are comparable. An HD molecule that is strongly backscattered moves more slowly in the laboratory frame than do molecules that are either sideways or forward scattered. Differential cross sections of the $D+H_2$ reaction vary with j'; the HD product is strongly backscattered at low j' and sidescattered at high j'.[18] Consequently, under conditions in which the products have sufficient translational energy that significant product fly-out from the probe volume and/or extraction slit area occurs, the detection procedure will discriminate against high j' states.

For the PLP geometry the test for detection-volume fly-out involved measuring rotational distributions for the reaction $D+H_2(v=0,j)\rightarrow HD(v'=0,j')+H$ using two experimental geometries with similar values of E_{rel} ($\lambda_{photolysis}$): the PLP arrangement ($\lambda_{photolysis}\approx 204$ nm) and an ILP setup ($\lambda_{photolysis}=202.5$ nm) in which the photolysis beam was approximately 3 mm in diameter. The 202.5 nm light for the ILP setup was generated using the fourth harmonic of the Nd:YAG laser (266 nm) mixed in BBO with 848 nm light from a dye laser. Product fly-out was negligible for the expanded reaction volume associated with the ILP geometry, as demonstrated in previous experiments.[7,12,13] The two distributions are nearly identical [Fig. 6(a)], which demonstrates that detection-volume fly-out was insignificant in the PLP geometry.

For the ILP geometry the test for detection-volume fly-out entailed using two different photolysis conditions: a focused photolysis beam and a 3 mm photolysis beam. In both cases, the photolysis source was the fifth harmonic of the Nd:YAG laser ($\lambda_{photolysis}=212.8$ nm). Rotational distributions for the reaction $D+H_2(v=0,j)\rightarrow HD(v'=0,j')+H$ were recorded. Very good agreement was found between the focused and collimated photolysis-source experiments [Fig. 6(b)], demonstrating that fly-out was not influencing our measurements in the ILP geometry.

To check for HD^+ ion-extraction loss, the slit width was increased by more than a factor of 2. Excellent agreement was observed between distributions for the reaction $D+H_2(v=0,j)\rightarrow HD(v'=0,j')+H$ recorded with the enlarged (7 mm) and normal (3 mm) extraction slit widths, as shown in Fig. 7. Hence, HD^+ ions were not lost during the extraction process. We conclude that HD product fly-out did not contribute a systematic error to the measured HD internal-state distributions.

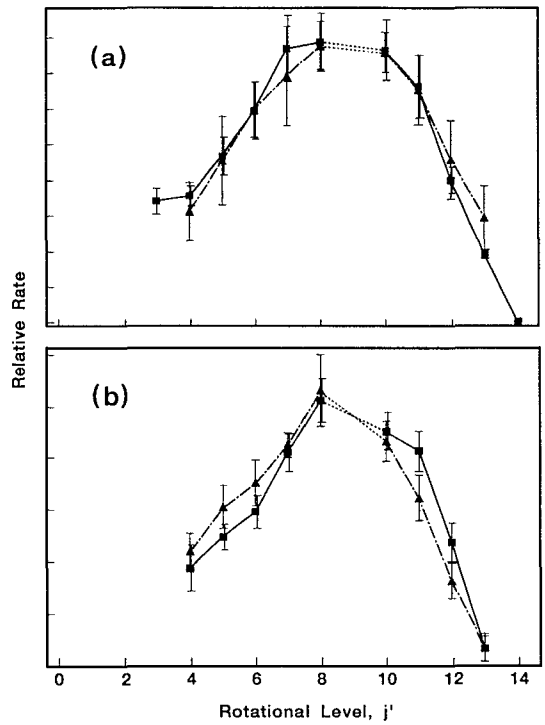

FIG. 6. Comparison of the $D+H_2(v=0,j)\rightarrow HD(v'=0,j')+H$ product rotational distributions: (a) at $E_{rel}=1.5$ eV obtained with a 3 mm diameter photolysis beam using an ILP geometry (squares connected by solid lines) and a PLP geometry (triangles connect by dashed-dotted-dashed lines), and (b) at $E_{rel}=1.35$ eV obtained with a 3 mm diameter photolysis beam using an ILP geometry (squares connected by solid lines) and a focused beam ILP geometry (triangles connected by dashed-dotted-dashed lines). Error bars represent one standard deviation.

5. ILP time delay study

The time delay between the photolysis and probe laser pulses, Δt (Sec. II A 1 and II D), must be sufficiently long that an observable concentration of HD is formed but short enough to avoid product fly-out, reagent $H_2(v=1, j=1)$ fly-out for the SRP distributions, and collisional relaxation of reactants and products. In the preceding section we showed that product fly-out was negligible. In addition, the short time delays associated with these measurements eliminate reagent or product collisional relaxation;[7,12,13] thus, the time-delay study was primarily a test for $H_2(v=1, j=1)$ fly-out. Partial $HD(v'=1,j')$ rotational distributions were recorded for the $D+H_2(v=0,j)$ and $D+H_2(v=1, j=1)$ reactions for $\Delta t=15$, 20, 28, 35 ns. No change in the distributions was observed for reaction with $H_2(v=0,j)$, as expected; however, for reaction with $H_2(v=1, j=1)$ a significant change in the distributions was found (Fig. 8). The relative rates into high j' states decreased as Δt increased.

This perturbation of the rotational distribution was caused by $H_2(v=1, j=1)$ leaving the probe volume follow-

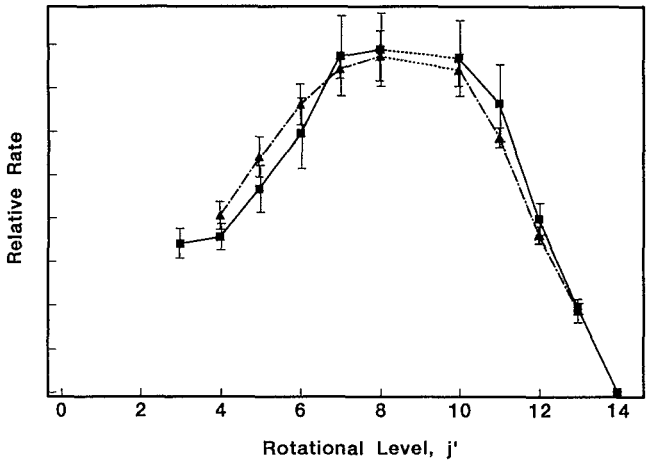

FIG. 7. Comparison of the $D+H_2(v=0,j)\rightarrow HD(v'=0,j')+H$ product rotational distributions obtained using a PLP geometry, but with a 3 mm extraction slit width (squares connected by solid lines) and a 7 mm extraction slit width (triangles connected by dashed-dotted-dashed lines). Error bars represent one standard deviation.

ing SRP, leading to a time-dependent concentration of $H_2(v=1,j=1)$. The contribution from the ILP reaction to the ion signal was not affected by this decrease because the time delay between the photolysis and SRP pulses was fixed at 15 ns, a delay at which fly-out was determined to be negligible (Sec. II B 4). The contribution from the probe-laser-induced reaction to the ion signal that we subtract out using an every-other-shot subtraction procedure (Sec. II A 1), however, was affected by this decrease because the subtraction procedure entailed switching the probe laser between two values of Δt; $H_2(v=1,j=1)$ fly-out could not be neglected for the longer time delay. Using REMPI we determined that $[H_2(v=1,j=1)]$ decreased by 2–5 % between the short ($\Delta t=7$ ns) and long ($\Delta t=20$ ns) delays, whereas it decreased by 6–9 % when $\Delta t=28$ ns for the long delay.

For product rotational levels in which there was a significant enhancement in reaction rate upon SRP (i.e., high j') the decrease in $[H_2(v=1,j=1)]$ at the longer delay caused the subtraction procedure to overcompensate for the PLP ion signal. The overcompensation was more marked at high j' because the enhancement in the rate upon vibrational excitation of the reagent was the greatest for these levels. This explanation accounts for the observed depletion in the relative rates of the high j' states as Δt was increased (Fig. 8).

Given the good agreement between the $\Delta t=15$ and 20 ns partial distributions and the small change in SRP efficiency at these time delays, we do not expect the systematic error associated with this effect to exceed significantly the statistical fluctuations in these measurements. An approximate measure of this error was determined by linear interpolation of the results of the time delay study. The average value of the change in the $j'=8$ relative rate with Δt was 0.94%/ns. This value was used to extrapolate from the longer ($\Delta t=20$ ns) to the shorter ($\Delta t=7$ ns) delay, predicting a 12% change in the rate between these time delays. This estimate provides an upper bound because the time dependence of the reaction rate was determined at the most populated j' of the Raman-pumped distribution, where the relative rate was most sensitive to $[H_2(v=1,j=1)]$. The error bars presented in Fig. 12 for the $D+H_2(v=1,j=1)\rightarrow HD(v'=1,j')+H$ ILP distribution are a combination of this 12% systematic error and the measurement error (12% was added to the random error for each j'). The measurement error and the combined systematic and random error are presented in Table III.

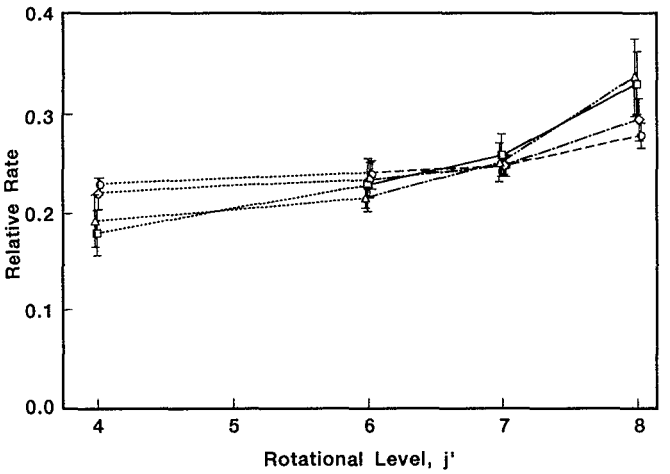

FIG. 8. Comparison of the partial $D+H_2(v=1,j=1)\rightarrow HD(v'=1,j')+H$ product rotational distributions for four time delays of the probe laser with respect to the photolysis laser: 15 ns (triangles connected by dashed-dotted-dotted-dashed lines), 20 ns (squares connected by solid lines), 28 ns (diamonds connected by dashed-dotted-dashed lines), and 35 ns (circles connected by dashed lines). Error bars represent one standard deviation.

C. DBr photolysis tests

In previous experiments using DBr photolysis, substantial D^+ ion production was observed.[9,13] The magnitude of the D^+ ion signal has a strong wavelength dependence, particularly in the 211–215 nm probe region, corresponding to $HD(v'=1;j'=8\text{–}11)$. For some j' levels, the arrival time of the HD^+ ions in the TOF/MS was distorted by the large D^+ peak. Recent measurements of the multiphoton ionization spectrum of HBr show significant H^+ ion production and a large degree of structure in the HBr spectrum.[44] These findings suggest that the D^+ ions arise from DBr ionization followed by fragmentation into D^+ and Br.

To determine if space-charge effects were distorting the measurements for the reaction $D+H_2(v=1,j=1)\rightarrow HD(v'=1,j')+H$, distributions were recorded using three mix ratios ($He:H_2:DBr$), 14:1:1, 20:3:1, and 41:6:1. Good agreement was observed among the distributions and with previously measured ones.[9,13]

In the previous studies of KZ and KAZ, the data-collection electronics were adjusted at each j' for the DBr experiments. As an additional check, we recorded distributions in which the temporal width of the gated integrator was increased to include the arrival time of all j' ion signals

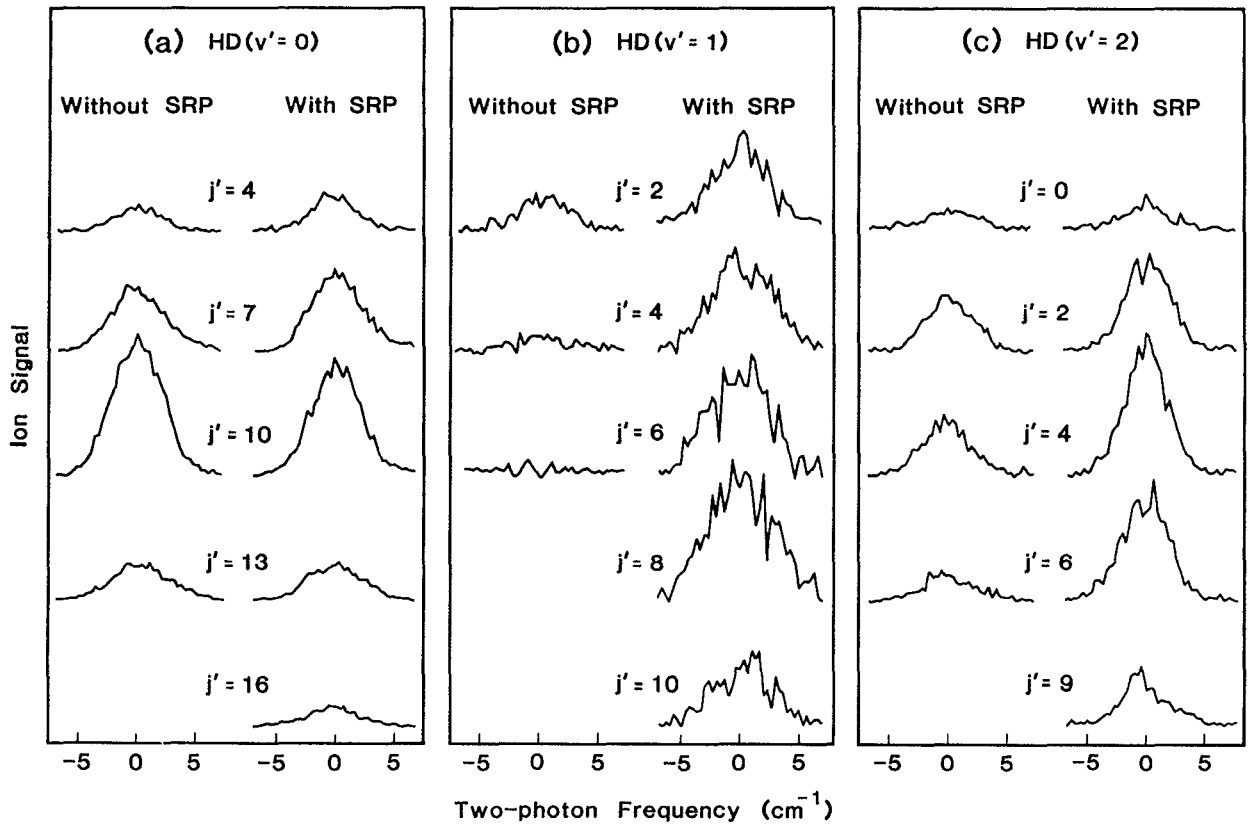

FIG. 9. Representative spectral peaks of the $D+H_2$ reaction for (a) $HD(v'=0,j')$ at $E_{rel}=1.5$ eV; (b) $HD(v'=1,j')$ at $E_{rel}=0.8$ eV, and (c) $HD(v'=2,j')$ at $E_{rel}=1.3$ eV products. The peaks in the left column were recorded without SRP and those in the right column with SRP. Each trace represents one scan, which took 90–240 s; see text for additional information on the experimental procedure. All peaks for a given figure were recorded on the same day. On the abscissa, 0 denotes line center.

and no adjustment of the electronics was made while recording the distributions. Once again, good agreement was found between the new and old data sets.

Using the ILP geometry and 266 nm photolysis of DI we could come close to the same E_{rel} as the previous DBr measurements. A comparison between the DBr experiments and the new ILP experiments is presented in Sec. IV.

D. Experimental procedure

We report three sets of HD product rotational distributions in which DI was the photolytic D-atom source and the H_2 reagent was either thermal or prepared in the ($v=1$, $j=1$) state. $HD(v'=0$ and $2;j')$ distributions were measured using the PLP setup, and the ILP geometry was used for the $HD(v'=1,j')$ rotational distribution; the $HD(v'=1,j')$ PLP distribution was previously reported.[13] We also determined vibrational product-state distributions and the enhancement of the rate into a specific product vibrational level upon vibrational excitation of the H_2 reagent. In addition, the product rotational distribution for the reaction $D+H_2(v=0,j)\rightarrow HD(v'=0,j')+H$ was measured using the ILP geometry and DI photolysis.

The experimental procedure for both the PLP and ILP geometries was the same as previously outlined.[13] The $D+H_2\rightarrow HD(v',j')+H$ product rotational distributions were recorded with and without SRP of the H_2 reagent 13–18 times on 4–5 separate days. On a given day, 2–5 pumped and/or 2–5 unpumped distributions were recorded. Representative spectral peaks for the $HD(v'=0$, 1, and 2) distributions with and without SRP are shown in Fig. 9. The peaks displayed in each panel were recorded on a single day, so their areas reflect the relative populations of the $HD(v',j')$ levels. The SRP efficiency was measured both before and after pumped distributions were recorded. Using the PLP geometry the fraction of vibrationally excited H_2 was $33.2\pm1.6\%$ for the measurement of the $HD(v'=0,j')$ distribution and $34.1\pm1.3\%$ for the $HD(v'=2,j')$ distribution. For the ILP geometry, the fraction of vibrationally excited H_2 was $31.6\pm1.3\%$ for the $HD(v'=1,j')$ distribution.

The $D+H_2(v=1,j=1)\rightarrow HD(v',j')+H$ state-to-state product rotational distributions were extracted from the measured distributions by subtracting the contributions of the $D+H_2(v=0)$ reaction from the SRP distributions. This procedure required knowledge of the relative magnitudes of the pumped and unpumped distributions, which was obtained by measuring the SRP enhancement of a specific rotational state within each $HD(v')$ level. The states used were $j'=12$ for $HD(v'=0)$, $j'=4$ for

$HD(v'=2)$, and $j'=7$ for $HD(v'=1)$. The pumped and unpumped distributions were "locked" in this manner each day that SRP distributions were recorded. The measured enhancements were 0.95 ± 0.05 for $HD(v'=0, j'=12)$, 2.2 ± 0.2 for $HD(v'=2, j'=3)$, and 5.8 ± 1.2 for $HD(v'=1, j'=4)$.

Determination of vibrational branching ratios for the PLP arrangement required that $HD(v'=1)$ be locked to $HD(v'=0)$ and $HD(v'=2)$. Locking two vibrational levels involved determining the relative rates into a given rotational state in each of the vibrational levels. $HD(v'=1, j'=12)$ and $HD(v'=2, j'=3)$ were used to lock $v'=1$ and 2, and $HD(v'=1, j'=4)$ and $HD(v'=0, j'=12)$ were used to lock $v'=0$ and 1. The vibrational levels were locked each day data for $v'=0$ or 2 were recorded.

The dichroic mirrors used to direct the probe beam into the vacuum chamber (Figs. 1 and 2) cover the spectral region 201–215 nm. This region includes $H_2(v=0, j=1)$, used for measurement of the SRP efficiency, and all of the $HD(v'=0,1,j')$ rotational distributions. For recording the $HD(v'=2,j')$ distribution a second set of dichroic mirrors was required. For these distributions the SRP efficiency was optimized and measured, the dichroics were changed, and the SRP efficiency was reoptimized at $HD(v'=1, j'=12)$. After $HD(v'=2,j')$ distributions were recorded the dichroic mirrors were changed back, the SRP efficiency remaximized at $HD(v'=1, j'=12)$, and the SRP efficiency remeasured. For a given day values of the initial and final SRP efficiencies agreed to within a few percent.

E. REMPI calibration

The REMPI-TOF/MS detection procedure has been calibrated against a high-temperature, effusive nozzle,[31] which provided correction factors to convert measured ion signals into relative quantum-state populations. Vibrational correction factors were measured, which permit vibrational product state distributions to be determined; $HD(v=0$, 1, and 2) have been calibrated. Moreover, rotational correction factors were determined; however, the range of calibrated rovibrational levels does not cover the range of levels measured in these experiments. The HD rovibrational levels calibrated were $(v=0, j=0$–$13)$, $(v=1, j=2$–$11)$, and $(v=2, j=2$–$8)$.

There are three types of entries in Tables I–IV and in Figs. 6, 7, and 10–17 as listed in the following:

(1) Calibrated or estimated populations. Calibrated populations use experimentally derived correction factors to relate ion signals to relative quantum-state populations, whereas estimated populations rely on theoretically derived correction factors, which are generally in very good agreement with the experimental values for the calibrated levels. For most of these levels the experimentally and theoretically derived correction factors are unity. These levels are denoted by entries in the tables without parentheses (solid squares in the figures).

(2) Uncalibrated populations. For these levels $(j'\geqslant 14)$, significant tunneling occurs in the E,F state, the intermediate state in the (2+1) REMPI detection scheme. The measured ion signals for these levels constitute lower limits on the actual populations. These entries are given in square brackets in the tables (open squares in the figures). These levels were included in the normalizations employed to compare the present distributions with theory and with other experimental results. They were also used to determine vibrational distributions.

(3) Omitted levels. HD impurity in the reagent H_2 resulted in contamination of thermally populated j' states. The product states affected were $HD(v'=0, j'=0$, 1, and 2), and populations of these levels were not measured. The $HD(v'=2, j'=1)$ spectral peak could not be recorded because it overlaps the $HD(v'=1, j'=15)$ spectral peak in the (2+1) REMPI detection scheme. Similarly, $HD(v'=0, j='15)$ and $H_2(v=1, j=1)$ are in close spectroscopic proximity, as are $HD(v'=0, j'=9)$ and the Lyman β transition for D. As a result of large, interfering ion signals $HD(v'=0, j'=15$ and 9) populations could not be measured and are omitted from tables and figures.

The integrated area of a REMPI spectral peak corresponds to the density of that quantum state; thus, the measured $HD(v',j')$ ion signal corresponds to the relative rate of reaction into that state. These rate constants are related to (average) cross sections via multiplication by the relative velocity of the reagents.[45]

III. RESULTS

A. Rotational distributions

We have measured product rotational distributions with SRP ("pumped") and without SRP ("unpumped"). To extract the $D+H_2(v=1, j=1)$ distribution from the measured ones, the pumped and unpumped distributions were locked so that the $D+H_2(v=0,j)$ component of the pumped distribution could be removed. Figure 10(a) shows the PLP $HD(v'=2,j')$ distribution at $E_{rel}=1.3$ eV measured with SRP (solid line) and without SRP (dashed line). By subtracting 65.9% of the unpumped from the pumped distribution, we obtained the $D+H_2(v=1, j=1)\rightarrow HD(v'=2,j')+H$ state-to-state distribution, Fig. 10(b). The 65.9% takes into account the 34.1% depletion of the $H_2(v=0)$ by SRP.

The results presented in Fig. 10 are listed in Table I. Corresponding PLP results for $HD(v'=0,j')$ at $E_{rel}=1.5$ eV appear in Fig. 11 and Table II, and the $HD(v'=1,j')$ ILP results at $E_{rel}=0.78$ eV are presented in Fig. 12 and Table III. The error bars associated with the reaction $D+H_2(v=1, j=1)\rightarrow HD(v'=0,j')+H$ at $E_{rel}=1.5$ eV are relatively large because of the minimal enhancement in the populations of these levels upon SRP (refer to Fig. 11). The $D+H_2(v=0,j)\rightarrow HD(v'=0,j')+H$ ILP rotational distribution at $E_{rel}=1.35$ eV is displayed in Fig. 16 and listed in Table IV. Error bars denote one standard deviation in all figures and tables; for the $HD(v'=1,j')$ ILP results, a 12% systematic error was added to the random error (Sec. II B 5). In Figs. 10(b), 11(b), and 12(b) the error bars include uncertainties in the measured distributions, in the measurement of the SRP efficiency (Sec. II D), and in the locking of the pumped and unpumped distributions (Sec. II D).

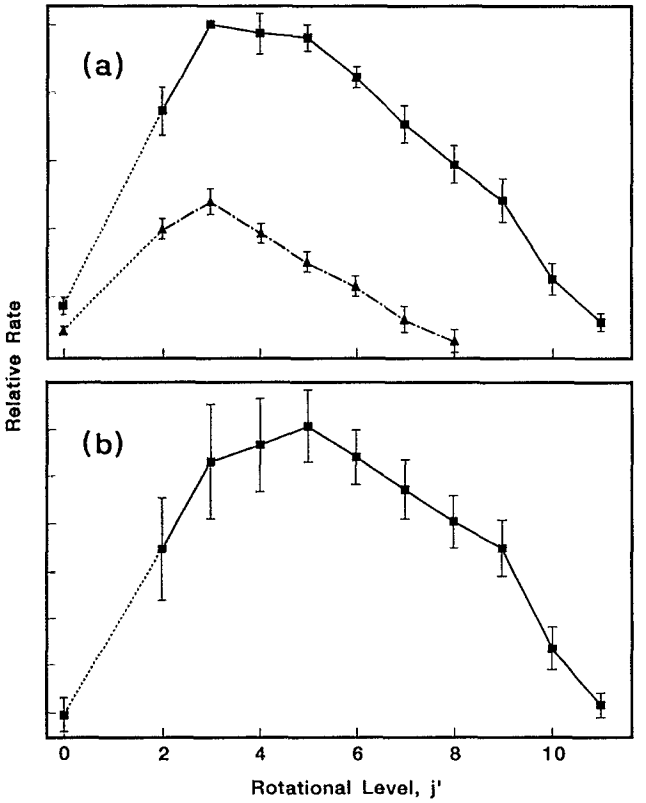

FIG. 10. Rotational distributions of the $HD(v'=2,j')$ product from the reaction $D+H_2$ at $E_{rel}=1.3$ eV. Error bars represent one standard deviation. (a) The unpumped distribution from the $D+H_2(v=0,j)$ reaction is represented by triangles connected by dashed-dotted-dashed lines. The pumped distribution in which 33% of the H_2 molecules were in the ($v=1$, $j=1$) state is represented by squares connected by solid lines. (b) The distribution from the reaction $D+H_2(v=1,j=1)$, which was obtained by subtracting ~67% of the unpumped distribution from the pumped distribution (refer to Sec. II D). Dotted lines connect the populations of levels adjacent to a level for which the population was not measured. Closed markers denote calibrated levels and open markers denote uncalibrated levels.

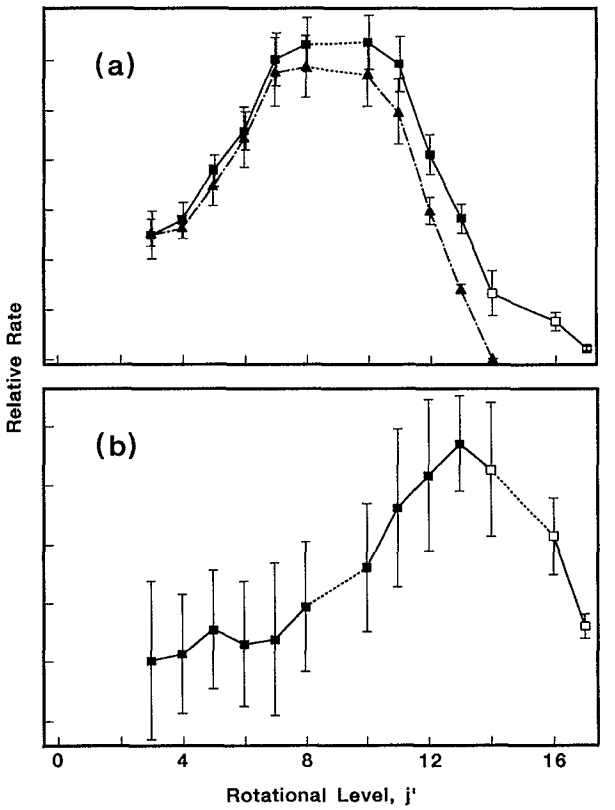

FIG. 11. Same as Fig. 10, but for the $HD(v'=0,j')$ product rotational distribution at $E_{rel}=1.5$ eV.

It was established previously[13] that the subtraction procedure is valid for the PLP reaction $D+H_2\rightarrow HD(v'=1,j')+H$ at $E_{rel}=1.0$ eV by demonstrating that the product rotational distribution for the reaction $D+H_2(v=0,j)\rightarrow HD(v'=1,j')+H$ was unperturbed by changing from *normal*-H_2 to *para*-H_2. Although the dependence of the $HD(v'=0,2;j')$ rotational distributions on the $H_2(v=0,j)$ rotational distribution was not measured, these product states are expected to exhibit the same insensitivity to the H_2 rotational distribution.

TABLE I. Product rotational distributions for the reaction $D+H_2(v,j)\rightarrow HD(v'=2,j')+H$ at $E_{rel}=1.3$ eV.

j'	Unpumped ($v=0,j$)	Pumped ($v=0,1$, $j=1$)	($v=1$, $j=1$)
0	0.05±0.007	0.025±0.004	0.012±0.005
1			
2	0.19±0.01	0.11±0.01	0.088±0.014
3	0.23±0.02	0.14±0.01	0.12±0.01
4	0.18±0.01	0.142±0.008	0.13±0.1
5	0.14±0.01	0.14±0.006	0.139±0.008
6	0.11±0.1	0.123±0.004	0.127±0.006
7	0.06±0.01	0.103±0.008	0.11±0.01
8	0.03±0.02	0.086±0.008	0.10±0.01
9		0.07±0.009	0.09±0.01
10		0.037±0.007	0.046±0.009
11		0.018±0.004	0.023±0.005

TABLE II. Product rotational distributions for the reaction $D+H_2(v,j)\rightarrow HD(v'=0,j')+H$ at $E_{rel}=1.5$ eV.

j'	Unpumped ($v=0,j$)	Pumped ($v=0,1$, $j=1$)	($v=1$, $j=1$)
0			
1			
2			
3	0.064±0.007	0.051±0.009	0.00±0.05
4	0.066±0.006	0.057±0.007	0.01±0.05
5	0.087±0.010	0.078±0.005	0.03±0.05
6	0.111±0.015	0.096±0.004	0.02±0.05
7	0.145±0.017	0.124±0.008	0.02±0.06
8	0.147±0.015	0.132±0.008	0.05±0.06
9			
10	0.143±0.016	0.133±0.006	0.08±0.06
11	0.125±0.016	0.126±0.008	0.13±0.07
12	0.074±0.007	0.089±0.009	0.16±0.06
13	0.036±0.002	0.061±0.006	0.19±0.04
14	[0.0006±0.0001]	[0.028±0.009]	[0.17±0.06]
15			
16		[0.018±0.005]	[0.11±0.03]
17		[0.005±0.002]	[0.03±0.01]

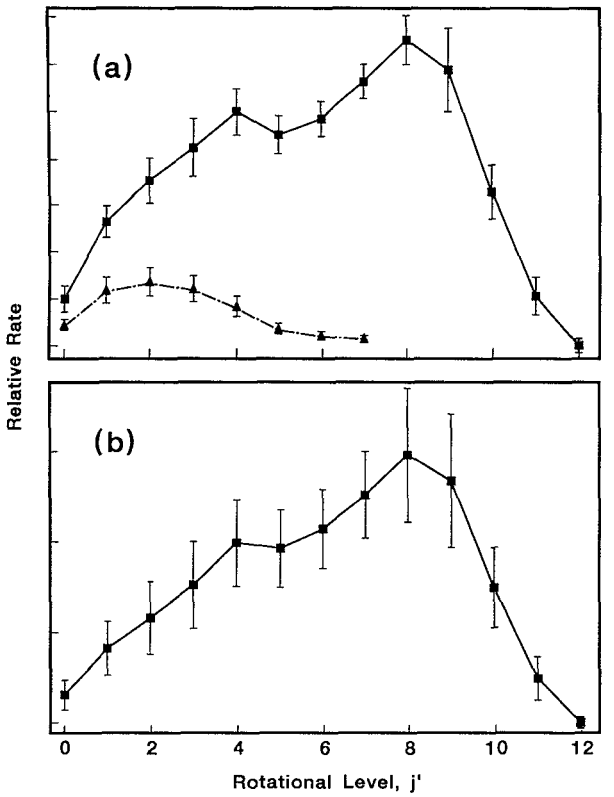

FIG. 12. Same as Fig. 10, but for the HD($v'=1,j'$) product rotational distribution at $E_{rel}=0.8$ eV.

The measured rotational distributions include most but not all of the energetically accessible HD(v',j') product states; the energetically accessible product states are (1) HD($v'=0$, $j'=0$–17), HD($v'=1$, $j'=0$–8), and HD($v'=2$, $j'=0$–9) for the reaction with $H_2(v=0,j)$, and (2) HD($v'=0$, $j'=0$–20), HD($v'=1$, $j'=0$–13), and HD($v'=2$, $j'=0$–14) for the reaction with $H_2(v=1, j=1)$. Each distribution is unimodal, allowing the populations of missing levels to be estimated. For the PLP rotational distributions ($E_{rel}\approx 1.4$ eV), the peak j' is negatively correlated with v'. In addition, the data show that reagent vibrational excitation results in substantial product rotational excitation for each v'.

TABLE III. Product rotational distributions for the reaction D +$H_2(v,j)$→HD($v'=1,j'$)+H at $E_{rel}=0.8$ eV.

j'	Unpumped ($v=0,j$)	Pumped ($v=0,1$, $j=1$)	($v=1$, $j=1$)[a]
0	0.078±0.019	0.021±0.006	0.015±0.009(0.007)
1	0.20±0.05	0.055±0.007	0.04±0.01(0.009)
2	0.23±0.05	0.07±0.01	0.06±0.02(0.01)
3	0.21±0.04	0.09±0.01	0.08±0.02(0.01)
4	0.15±0.04	0.10±0.01	0.10±0.02(0.008)
5	0.06±0.02	0.093±0.008	0.10±0.02(0.008)
6	0.035±0.017	0.100±0.008	0.11±0.02(0.007)
7	0.028±0.012	0.116±0.008	0.12±0.02(0.007)
8		0.13±0.01	0.15±0.04(0.02)
9		0.12±0.02	0.133±0.04(0.02)
10		0.07±0.01	0.07±0.02(0.01)
11		0.022±0.008	0.02±0.01(0.008)
12		0.00±0.003	0.00±0.004(0.003)

[a]Numbers in parentheses do not include the 12% $H_2(v=1, j=1)$ fly-out error.

TABLE IV. Product rotational distributions for the reaction D +$H_2(v,j)$→HD($v'=0,j'$)+H at $E_{rel}=1.35$ eV.

j'	Population
0	
1	
2	
3	
4	0.078±0.012
5	0.094±0.006
6	0.107±0.008
7	0.14±0.01
8	0.17±0.01
9	
10	0.15±0.01
11	0.14±0.01
12	0.09±0.01
13	0.036±0.006

B. Vibrational branching ratios and enhancements

Two approximations were necessary to calculate vibrational branching ratios because not all of the energetically accessible rovibrational states were measured. For the three levels where measurement was not possible [i.e., HD($v'=0, j'=9,15$), and HD($v'=2, j'=1$)], populations were determined by linear interpolation between the two adjacent levels, and populations were assumed to be zero for states beyond the range of the measured distributions. These approximations are not expected to affect substantially the calculated values. The vibrational distributions are presented in Fig. 13 and Table V.

The locking of the pumped and unpumped distributions is preserved through the subtraction procedure. The enhancement of the HD(v') reaction rate that occurs upon reagent vibrational excitation may therefore be calculated according to

$$\frac{k_{1v'}}{k_{0v'}}=\sum_{j'}P(v=1,j=1;v',j')/\sum_{j'}P(v=0,j\ \text{thermal};v',j'), \tag{2}$$

where $k_{vv'}$ denotes the rate of the reaction D +$H_2(v,j)$→HD(v', all j')+H and P($v,j;v',j'$) is the relative population of the HD(v',j') product level when the H_2 reagent is initially in the rovibrational state (v,j). Tables VI–VIII give the values of the vibrational enhancements for HD($v'=0$), HD($v'=1$), and HD($v'=2$), respectively.

As shown in Fig. 13, the product vibrational distribution is strongly peaked at $v'=0$ for the reaction with $H_2(v=0,j)$, whereas $v'=0$ and 1 are comparable for the reaction with $H_2(v=1, j=1)$. Reagent vibrational excitation increases the total energy by approximately 0.5 eV and allows the H_2 bond to be highly elongated; the $H_2(v=1)$ outer turning point has an internuclear distance 0.26 Å greater than the $H_2(v=0)$ equilibrium bond length.[46] Ini-

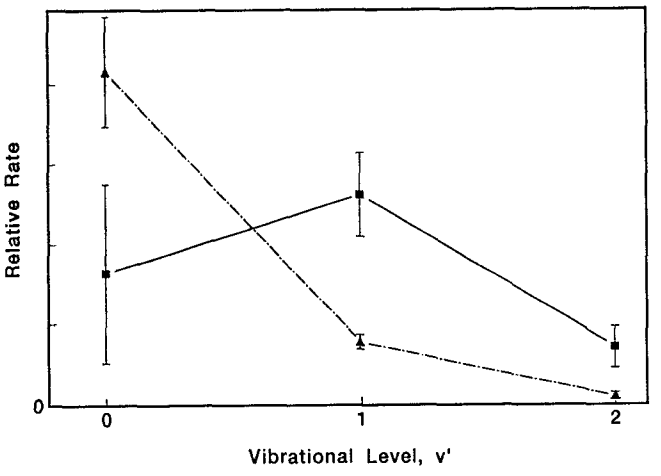

FIG. 13. Vibrational state distribution of the HD product of the D+H_2 reaction. Triangles connected by dashed-dotted-dashed lines denote the distribution from the D+$H_2(v=0,j)$ reaction and squares connected by dashed lines denote the distribution from the D+$H_2(v=1, j=1)$ reaction. Error bars represent one standard deviation.

tially, we were surprised to find that the total reaction rate changes little, if at all, upon reagent vibrational excitation (Table X). Because the collision time is shorter than the vibrational period, reactive collisions average different nuclear configurations of the H_2 reagent. In this regard it is interesting to note that the average nuclear separation in $H_2(v=1)$ is not much larger than that in $H_2(v=0)$.

C. Energetics

Tables VI–X summarize the partitioning of the available energy, E, among the degrees of freedom of the products of the reactions D+$H_2(v=0,j)$ and D+$H_2(v=1, j=1)$. The available energy is the sum of the relative collision energy, the reagent internal energy, and the reaction exothermicity. The reagent internal energy was 103 cm^{-1} for the D+$H_2(v=0,j)$ reaction [the average rotational energy corresponding to $H_2(v=0,j)$ at 150 K] and 4274 cm^{-1} for the D+$H_2(v=1, j=1)$ reaction. The first moments, $\langle j' \rangle_{v'}$, and rotational energy partitioning factors, $f_R(v')$ and $g_R(v')$, were calculated for each of the distributions measured, as were the fractions of E partitioned into product vibration, $f_{v'}$, and translation, f_T. The formulas used were:[45]

$$\langle j' \rangle_{v'} = \sum_{j'} j' P(v,j;v',j'), \tag{3}$$

TABLE V. Product vibrational distributions for the reaction D+$H_2(v,j)\rightarrow$HD(v',j')+H at $E_{rel}\approx 1.4$ eV.

v'	$(v=0,j)$	$(v=1, j=1)$
0	0.83±0.14	0.32±0.22
1	0.15±0.02	0.52±0.10
2	0.018±0.007	0.14±0.05

TABLE VI. Energy-disposal parameters for the reaction D+$H_2(v,j)\rightarrow$HD$(v'=2,j')$+H at $E_{rel}=1.3$ eV.

	Experiment		QM calculations[a]	
	$(v=0,j)$	$(v=1, j=1)$	$(v=0,j)$	$(v=1, j=1)$
E (cm^{-1})	10 870	15 070		
$\langle j' \rangle$	3.6±0.1	5.4±0.3	3.4	5.5
f_R	0.074±0.006	0.108±0.005	0.066	0.11
g_R	0.21±0.02	0.20±0.01	0.19	0.21
k_{10}/k_{00}	7.8±1.4		10	

[a]Taken from Ref. 26.

$$g_R(v') = \sum_{j'} P(v,j;v',j') E_{v'}(j')/[E-E(v')], \tag{4}$$

$$f_R(v') = \sum_{j'} P(v,j;v',j') E_{v'}(j')/E, \tag{5}$$

$$f_{v'} = \sum_{v'} P(v') E(v')/E, \tag{6}$$

and

$$f_T = 1 - f_{v'} - \sum_{v'} P(v') f_R(v'), \tag{7}$$

where $E_{v'}(j')$ $[E(v')]$ is the rotational (vibrational) energy and $P(v,j;v',j')$ $[P(v')]$ is the relative population of the HD(v',j') [HD(v')] product level for the reaction D+$H_2(v,j)\rightarrow$HD(v',j')+H. The normalizations assumed in Eqs. (3)–(7) are

$$\sum_{v'} P(v') = 1 \tag{8a}$$

and

$$\sum_{j'} P(v,j;v',j') = 1. \tag{8b}$$

The approximations described in Sec. III B were used in the above calculations. In addition, the higher E_{rel} associated with the ground-state I channel was used to calculate E. We believe that this is a reasonable approximation because the fast D-atom channel was dominant for HD$(v'=0$ and 1) product states. At the photolysis wavelengths corresponding to HD$(v'=2)$ product states, comparable fractions of fast and slow D atoms were generated. The HD$(v'=2)$ product states were just barely energeti-

TABLE VII. Energy-disposal parameters for the reaction D+$H_2(v,j)\rightarrow$HD$(v'=0,j')$+H at $E_{rel}=1.5$ eV.

	Experiment		QM calculations[a]	
	Unpumped $(v=0,j)$	Pumped $(v=1, j=1)$	$(v=0,j)$	$(v=1, j=1)$
E (cm^{-1})	12 330	16 520		
$\langle j' \rangle$	8.1±0.3	12±2	8.5	12.2
g_R	0.28±0.01	0.43±0.06	0.31	0.44
k_{10}/k_{00}	0.41±0.28		0.77	

[a]Taken from Ref. 26.

TABLE VIII. Energy-disposal parameters for the reaction D $+H_2(v,j)\rightarrow HD(v'=1,j')+H$ at $E_{rel}=0.8$ eV.

	Experiment		QM calculations[a]	
	$(v=0,j)$	$(v=1,j=1)$	$(v=0,j)$	$(v=1,j=1)$
E (cm^{-1})	6680	10 870		
$\langle j'\rangle$	2.6±0.2	6.9±0.3	2.2	6.9
f_R	0.077±0.007	0.20±0.01	0.06	0.23
g_R	0.17±0.02	0.30±0.02	0.13	0.34
k_{10}/k_{00}	22±2		19.8	

[a]Taken from Ref. 26.

cally accessible to reactive collisions involving slow D atoms; consequently, D atoms from the fast channel made the major contribution to reaction.

IV. DISCUSSION

As described earlier, photolysis of DI generated fast D atoms, stimulated Raman pumping prepared the H_2 reagent in the state $(v=1, j=1)$, and (2+1) resonance-enhanced multiphoton ionization detected the nascent HD product in a quantum-state-specific manner. Using this procedure we have measured the relative rates of formation of $HD(v'=0,1,2;j')$ for the reactions of D+$H_2(v=0,j)$ and D+$H_2(v=1, j=1)$. In this section, we describe the internal-state distributions (Sec. IV A), evaluate the reliability of DBr as a fast D-atom precursor (Sec. IV B), and compare our results with QM calculations that fully simulate the experimental conditions (Sec. IV C). As mentioned in the experimental section (Sec. II A 3.), the photolysis of DI(DBr) leads to D atoms with two different energies, which correspond to the production of the halogen atom in its two spin–orbit states. As a shorthand we give the E_{rel} value of the fast D-atom channel only because fast D atoms were the dominant photolysis product and made the major contribution to reaction.

A. Product state distributions

It might be thought that the effect of vibrational excitation of the H_2 reagent is to present a larger target to the incoming D atom and to permit reactions with more bent geometries, i.e., that the "cone of acceptance" for the reaction may be increased upon reagent vibrational excitation.[9,13,46] This picture predicts that reagent translation would be channeled into product rotation more efficiently for D+$H_2(v=1, j=1)$ than for the ground-state reaction and that the total reaction rate would increase. A detailed examination of our results does not confirm this simple picture. Instead, we are led to a model in which internal energy of the reagent appears as internal energy of the product, while translational energy of the reagent is converted primarily into translation of the product. We call this model the conservation of internal energy (CIE) model.

To test the validity of the CIE model, we examine the fraction of reagent translation that appears as product translation. For the reaction D+$H_2(v=0,j)$ the fraction of available energy that appears in product translation, f_T, is 0.68 (Table X). In this reaction 98% of the available energy is from reagent translation and 2% from the change in zero-point energy and reagent internal energy. Thus, for the reaction D+$H_2(v=0,j)$, we find that ~70% of the reagent translational energy (E_T) appears in product translation ($E_{T'}$), i.e., $E_{T'}=0.70\ E_T$. For the reaction D $+H_2(v=1, j=1)$, f_T is 0.55, and 74% of the available energy originates as reagent translation. If we assume that reagent vibrational energy is converted exclusively into product internal energy, then $E_{T'}=0.74E_T$. Therefore, our data suggest that reagent vibrational excitation does not enhance the conversion of reagent translation into product internal energy. The apparent lack of coupling of reagent vibrational energy into product translation is consistent with previous experiments[47] and calculations[18,48,49] that find the reaction D+$H_2(v=1, j=1)$ to be moderately vibrationally adiabatic; this effect is related to the symmetric location of the reaction barrier on the H_3 potential energy surface (PES).[1,45]

The lack of enhancement in the conversion of reagent translation into product internal energy upon reagent vibrational excitation is also evident from comparisons of the fraction of E appearing in product rotation for a given product vibrational state, $g_R(v')$. For reactions with the same change in vibrational state from reactants to products, Δv, we find that the $g_R(v')$ values agree within experimental uncertainty for two sets of reactions: (a) D+$H_2(v=0,j)\rightarrow HD(v'=0)+H$ and D+$H_2(v=1, j=1)\rightarrow HD(v'=1)+H$ and (b) D+$H_2(v=0,j)$ $\rightarrow HD(v'=1)+H$ and D+$H_2(v=1, j=1)\rightarrow HD(v'=2)$ $+H$. The $g_R(v')$ values are (a) $g_R(v'=0)=0.28\pm0.01$ and $g_R(v'=1)=0.27\pm0.02$, and (b) $g_R(v'=1)=0.197$ ±0.006 and $g_R(v'=2)=0.20\pm0.01$. Using the CIE

TABLE IX. Energy-disposal parameters for the reaction D $+H_2(v,j)\rightarrow HD(v'=1,j')+H$ at $E_{rel}=1.4$ eV.

	Experiment[a]		QM calculations[b]	
	$(v=0,j)$	$(v=1,j=1)$	$(v=0,j)$	$(v=1,j=1)$
E (cm^{-1})	11 680	15 690		
$\langle j'\rangle$	5.2±0.1	7.9±0.4	5.1	9.2
f_R	0.136±0.004	0.21±0.01	0.134	0.259
g_R	0.197±0.006	0.27±0.02	0.19	0.34
k_{10}/k_{00}	3.4±0.2		3.8	

[a]Taken from Ref. 13.
[b]Taken from Ref. 26.

TABLE X. Overall energy-disposal parameters for the reaction D $+H_2(v,j)\rightarrow HD(v',j')+H$ at $E_{rel}\approx1.4$ eV.

	Experiment		QM calculations[a]	
	$(v=0,j)$	$(v=1,j=1)$	$(v=0,j)$	$(v=1,j=1)$
f_R	0.25±0.04	0.27±0.12	0.17	0.27
$f_{v'}$	0.06±0.02	0.18±0.08	0.053	0.16
f_T	0.69±0.06	0.55±0.20	0.78	0.57
$k_{1v'}/k_{0v'}$	1.0±0.5		1.4	

[a]Taken from Ref. 26.

model, this similarity is understandable because such pairs of reactions have comparable excess vibrational energies. This result is particularly interesting because the reactions in each pair sample very different regions of the PES.

We find that the total reaction rate into $HD(v'=0,1,2)$ does not increase upon vibrational excitation of H_2 (Table X). In contrast to the cone-of-acceptance picture, the CIE model does not require broadening of the overall opacity function. Apparently, the total energy of the system is sufficiently high that the added energy associated with H_2 vibration has virtually no effect on the reaction rate.

Additional support for the CIE model is provided by the measured increase in $f_{v'}$ and $g_R(v')$ upon reagent vibrational excitation (Tables VI–X). Compare $g_R(v')$ values for two $HD(v'=1,j')$ distributions with approximately the same total energy ($E_{tot}\approx 1.4$ eV): (1) $E_{rel}=0.8$ eV with vibrationally excited H_2, and (2) $E_{rel}=1.4$ eV with ground-state H_2. The $g_R(v'=1)$ values are 0.30 ± 0.02 and 0.197 ± 0.004 for reactions 1 and 2, respectively; that is, transfer of approximately 0.5 eV from reagent translation to vibration causes a 52% increase in $g_R(v')$. Similarly, $f_{v'}$ is 0.18 ± 0.08 for the reaction with $H_2(v=1,j=1)$ and f_v is 0.06 ± 0.02 for the reaction with $H_2(v=0,j)$. Thus, as the CIE model would predict, vibrational excitation of the reagent leads primarily to internal excitation of the product.

The increase in $g_R(v')$ upon H_2 vibrational excitation, $\Delta g_R(v')$, diminishes as v' is increased. The PLP measurements of $HD(v'=0,1,2;j')$ at $E_{rel}\approx 1.4$ eV demonstrate this decrease: $\Delta g_R(v'=0)=53\%$, $\Delta g_R(v'=1)=37\%$, and $\Delta g_R(v'=2)=0\%$. The CIE model predicts that the enhancement in $g_R(v')$ upon reagent vibrational excitation arises exclusively from the conversion of reagent vibration into product rotation. For higher product vibrational states less energy is available to couple into product rotation and, consequently, $\Delta g_R(v')$ decreases.

Our results are consistent with conservation of internal energy between reagents and products, and they indicate that conversion of reagent translation into product internal energy is not enhanced upon vibrational excitation of H_2. Whether this model is applicable to reactions of $D+H_2(v>1)$ would be interesting to determine.

B. Evaluation of the DBr photolytic precursor

As discussed in previous publications[9,13] and in Section II C, substantial D^+ ion production was observed for photolysis of DBr in the spectral region 211–215 nm, corresponding to $HD(v'=1, j'=8\text{–}11)$ for the PLP geometry. Because the discrepancy between QM theory[19,23,25] and experiment for the DBr/PLP reaction $D+H_2(v=1, j=1)\rightarrow HD(v'=1,j')+H$ is most pronounced in this range of j', several experimental checks were performed to evaluate the reliability of the DBr photolytic precursor. These checks included measurement of the probe-laser power dependence for j' levels within and outside of this region (Ref. 13 and Sec. II B 3); variation of the $He:H_2:DBr$ mix ratio, which varied the DBr density by a factor of 3 (Ref. 13 and Sec. II C), and investigation of different settings for the data-collection electronics (Sec. II C). No systematic errors were found by these measurements. The experimental checks provided necessary but

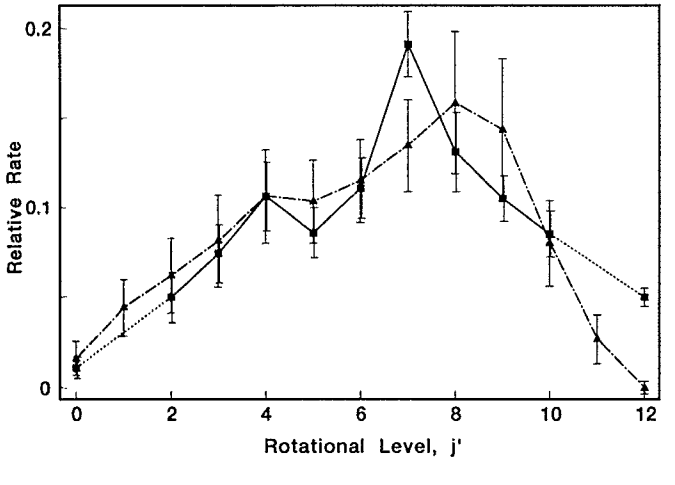

FIG. 14. Comparison of the $D+H_2(v=1, j=1)\rightarrow HD(v'=1,j')+H$ product rotational distributions obtained using the PLP geometry and DBr photolysis (squares connected by solid lines) with those obtained using the ILP geometry and DI photolysis (triangles connected by dashed-dotted-dashed lines). Error bars represent one standard deviation.

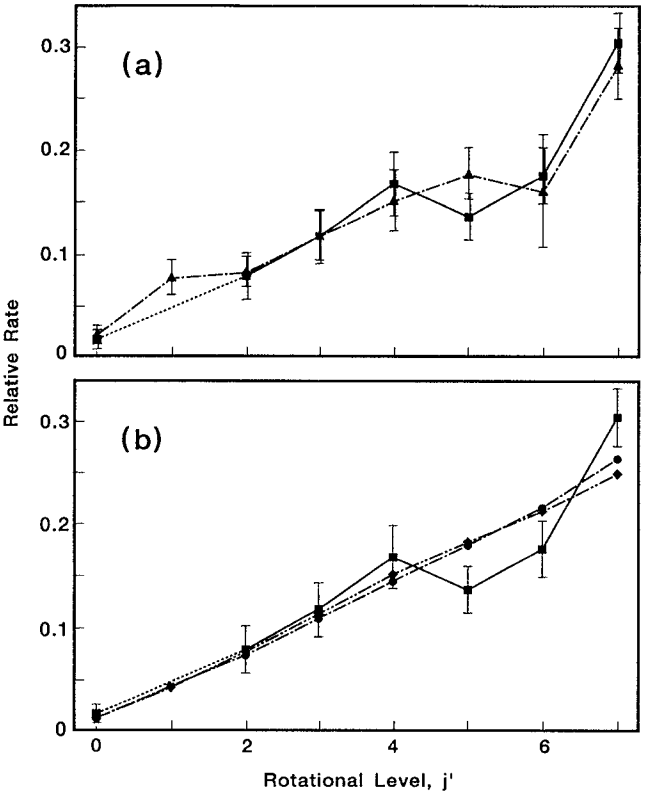

FIG. 15. Comparison of the truncated $D+H_2(v=1, j=1)\rightarrow HD(v'=1, j'=0\text{–}7)+H$ product rotational distributions obtained using the PLP geometry with DBr photolysis (squares connected by solid lines) with those of (a) the ILP geometry with DI photolysis (triangles connected by dashed-dotted-dashed lines), and (b) the calculations of Mielke *et al.* (Ref. 19) (diamonds connected by dashed-dotted-dotted-dashed lines) and of NJK (Ref. 26) (circles connected by dashed-dotted-dashed lines). Error bars represent one standard deviation.

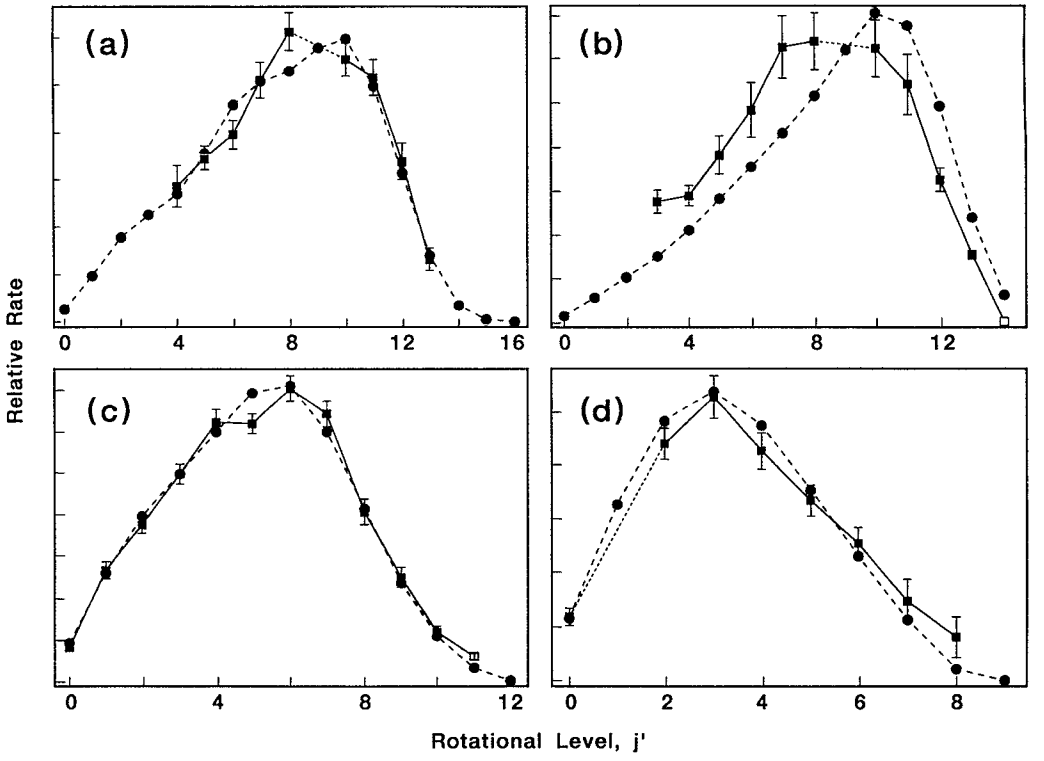

FIG. 16. Comparison of experimental (squares connected by solid lines) and quantum-mechanical (circles connected by dashed lines) rotational population distributions of the $HD(v',j')$ product of the $D+H_2(v=0,j)$ reaction for (a) $HD(v'=0)$ at $E_{rel}=1.35$ eV; (b) $HD(v'=0)$ at $E_{rel}=1.5$ eV; (c) $HD(v'=1)$ at $E_{rel}=1.4$ eV; (d) $HD(v'=2)$ at $E_{rel}=1.3$ eV. Error bars represent one standard deviation. Dotted lines connect the populations of levels adjacent to a level for which the population was not measured. For the experimental distribution, closed markers denote calibrated levels and open markers denote uncalibrated levels.

not sufficient evidence to conclude that DBr is a reliable photolytic precursor at these wavelengths.

The new ILP geometry provides an additional method to test the previous DBr/PLP measurements. This geometry with DI photolysis generates an E_{rel} value of 0.8 eV, which is nearly equal to the DBr/PLP value of 1.0 eV. D^+ ion production and consequent space-charge effects were nearly absent when DI was used as the photolytic precursor. In addition, the DI/ILP measurement is superior to the DBr/PLP measurement because the former has the advantages of a fixed photolysis wavelength (constant E_{rel} and I*/I) and accurately determined values for the I*/I branching ratio.[36] Figure 14 compares the DBr/PLP and DI/ILP product rotational distributions for the reaction $D+H_2(v=1,\ j=1)\rightarrow HD(v'=1,j')+H$. Good overall agreement is found between these distributions and the corresponding energy-disposal parameters, $\langle j'\rangle_{v'=1}$, f_R, and $g_R(v'=1)$ (Table VIII). The shapes of the two distributions are somewhat different, however, and the $E_{rel}=0.8$ eV (DI/ILP) distribution is slightly "hotter" than the $E_{rel}=1.0$ eV (DBr/PLP) distribution.

A more significant discrepancy exists between the two measurements for the enhancement of the rate into $v'=1$ upon reagent vibrational excitation (k_{11}/k_{01}, Table VIII): k_{11}/k_{01} is larger at $E_{rel}=0.8$ eV than at $E_{rel}=1.0$ eV by nearly a factor of 5. The DI/ILP data (Tables XIII and IX) indicate that this ratio is extremely sensitive to E_{rel}, which complicates comparisons of k_{11}/k_{01}. Assuming that k_{11}/k_{01} is a linear function of E_{rel}, interpolation of k_{11}/k_{01} for the DI experiments at $E_{rel}=0.8$ and 1.4 eV yields $k_{11}/k_{01}=12$ at $E_{rel}=1.0$ eV, in marked disagreement with the DBr/PLP measured value of 4.2 ± 0.3. Incidentally, the sensitivity to E_{rel} noted above demonstrates the importance of fully simulating the experimental initial conditions in comparisons between theory and experiment, at least for k_{11}/k_{01}.

As mentioned earlier, $HD(v'=1,j'=8)$ is at the onset of the perturbed spectral region in the DBr PLP experiment. If the previous DBr/PLP product distribution for the reaction $D+H_2(v=1,\ j=1)\rightarrow HD(v'=1,j')+H$ is truncated at $j'=7$, i.e., prior to the onset of the perturbed spectral region, excellent agreement is obtained between the DBr/PLP and DI/ILP truncated rotational distributions [Fig. 15(a)]. We conclude that DBr is not a reliable photolytic precursor in the PLP geometry for $HD(v'=1,\ j'\geqslant 8)$ in applications requiring quantitative determination of relative rates. This conclusion has almost no bearing on the reaction $D+H_2(v=0,j)\rightarrow HD(v'=1,j')+H$, for which $\sim 98\%$ of the product is formed in $j'<8$. It does, however, significantly limit the usefulness of the DBr/PLP measurements for the reaction $D+H_2(v=1,\ j=1)\rightarrow HD(v'=1,j')+H$. We were unable to identify the precise mechanism by which the measured populations of the $HD(v'=1,\ j'\geqslant 8)$ levels were perturbed. Reasonable

suggestions[13] include loss of product HD^+ ions because of space-charge effects and a decrease in concentration of the D-atom reagent because of D^+ ion production. Despite this lack of a positive, mechanistic identification, the onset of pathological behavior by the DBr precursor is experimentally evident in the TOF/MS detection procedure.

Finally, we compare the truncated DBr/PLP measurements with the QM calculations of Mielke *et al.*[19,25] and of NJK. Very good agreement is found between experiment and theory for both the rotational distributions [Fig. 15(b)] and the k_{11}/k_{01} ratio, where k_{11}/k_{01} is 2.1 ± 0.2 for the DBr/PLP experiment, 2.29 for Mielke *et al.*, and 2.35 for NJK. This comparison provides an admittedly limited test of the theoretical predictions at $E_{rel}=1.0$ eV because nearly half of the energetically accessible product levels are absent from the experimental distribution. Unfortunately, we do not anticipate being able to perform measurements that will provide a more rigorous test of these calculations. In the previous paper[13] we claimed there was a substantial discrepancy between theory and experiment. In light of the present findings, we are unable to make this claim based on the DBr/PLP experiments. The new DI/ILP and DI/PLP measurements are able, however, to provide a more complete and global test of QM theory (see below). We note that the remaining discrepancies between QM theory and experiment (Sec. IV C) are qualitatively similar to those found using the previous DBr/PLP measurements.

C. Comparison with QM calculations

NJK (Ref. 26) have performed QM calculations for the $D+H_2$ reaction over a broad range of energies, permitting a complete simulation of the experimental initial conditions; in particular, they included the variation in E_{rel} with rovibrational state probed for the PLP geometry, the experimental collision energy spread, and the fast and slow D-atom channels associated with X/X^* production, including the variation in this ratio with j' for the PLP experiments. For comparison, experimental and theoretical distributions have been normalized to the sum of the populations of their common levels. Experiment and theory are compared in Figs. 16–18. The experimental and predicted energy-disposal parameters are presented in Tables VI–X.

The level of agreement between the calculated and experimental results ranges from good to excellent. Quantitative agreement is found for the vibrational branching ratios (Fig. 18), $f_{v'}$ values (Table X), and the enhancement in the rate into a specific v' level upon vibrational excitation of the H_2 reagent (k_{11}/k_{01}, Tables VI–IX). Theory also quantitatively reproduces the PLP ($E_{rel}\approx1.4$ eV) rotational distributions and energy-disposal parameters for the reactions $D+H_2(v=0,j)\rightarrow HD(v'=1 \text{ and } 2;j')+H$ [Figs. 16(c) and (d)] and $D+H_2(v=1, j=1)\rightarrow HD(v'=2,j')+H$ [Fig. 17(d)]; and the ILP rota-

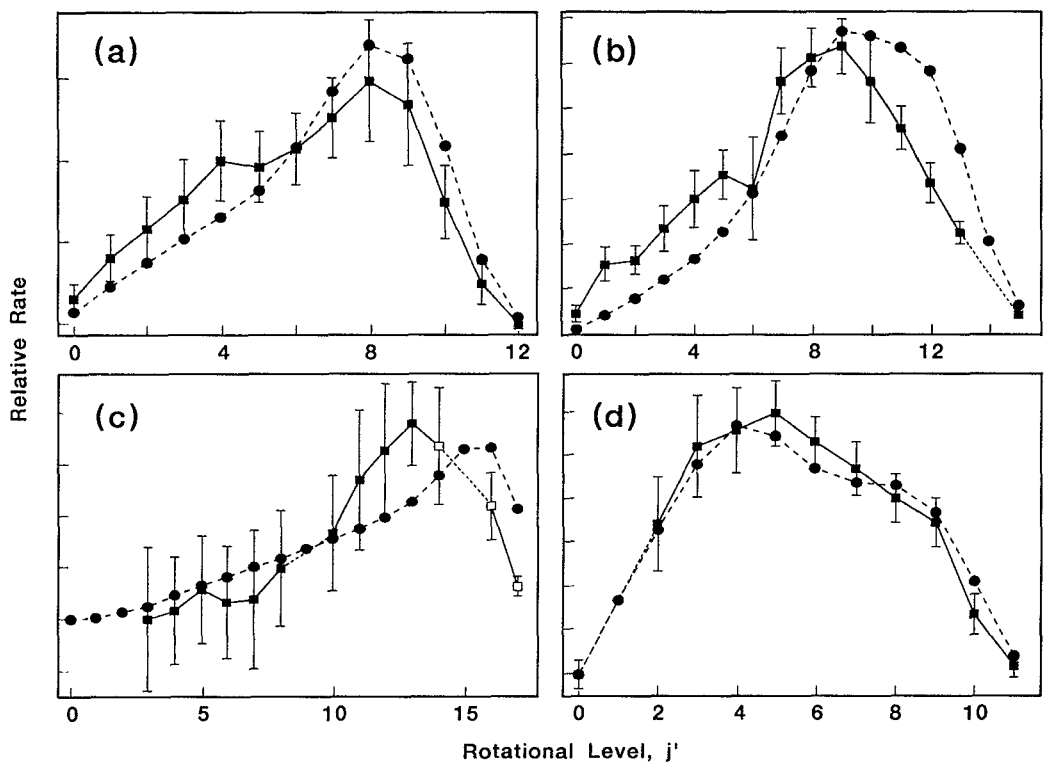

FIG. 17. Comparison of experimental (squares connected by solid lines) and quantum-mechanical (circles connected by dashed lines) rotational population distributions of the $HD(v'j')$ product for the $D+H_2(v=1, j=1)$ reaction: (a) $HD(v'=1)$ at $E_{rel}=0.8$ eV, (b) $HD(v'=1)$ at $E_{rel}=1.4$ eV, (c) $HD(v'=0)$ at $E_{rel}=1.5$ eV, (d) $HD(v'=2)$ at $E_{rel}=1.3$ eV. Error bars represent one standard deviation. Dotted lines connect the populations of levels adjacent to a level for which the population was not measured. For the experimental distribution, closed markers denote calibrated levels and open markers denote uncalibrated levels.

tional distributions and energy-disposal parameters for the reactions $D+H_2(v=0,j) \rightarrow HD(v'=0,j')+H$ at $E_{rel}=1.35$ eV [Fig. 16(a)] and $D+H_2(v=1, j=1) \rightarrow HD(v'=1,j')+H$ at $E_{rel}=0.8$ eV [Fig. 17(a)].

Significant differences persist between experiment and theory for $HD(v'=1)$ ($E_{rel}=1.4$ eV) and $HD(v'=0)$ ($E_{rel}=1.5$ eV) rotational distributions for the $D+H_2(v=1, j=1)$ reaction; see Fig. 17(b) and 17(c). Discrepancies are not limited to reactions in which H_2 was vibrationally excited, as comparable differences are observed for the $D+H_2(v=0,j) \rightarrow HD(v'=0,j')+H$ rotational distribution at $E_{rel}=1.5$ eV [Fig. 16(b)]. In contrast, for the same reaction at $E_{rel}=1.35$ eV, very good agreement is observed between the predicted and measured distributions [Fig. 16(a)]. Quantitative agreement also exists between the predicted and measured distributions for the reaction $D+H_2(v=1, j=1) \rightarrow HD(v'=2,j')+H$; see Fig. 17(d). The $HD(v'=0,j')$ distribution for the $D+H_2(v=1, j=1)$ reaction includes several rotational levels for which the REMPI detection scheme was not calibrated, unlike the other rotational distributions. Consequently, we judge the differences between theory and experiment to be less significant for this distribution. Nonetheless, we find that as the fraction of energy in product translation is increased, the experimental and theoretical results diverge; specifically, the predicted rotational distributions are "hotter" than the measured distributions.

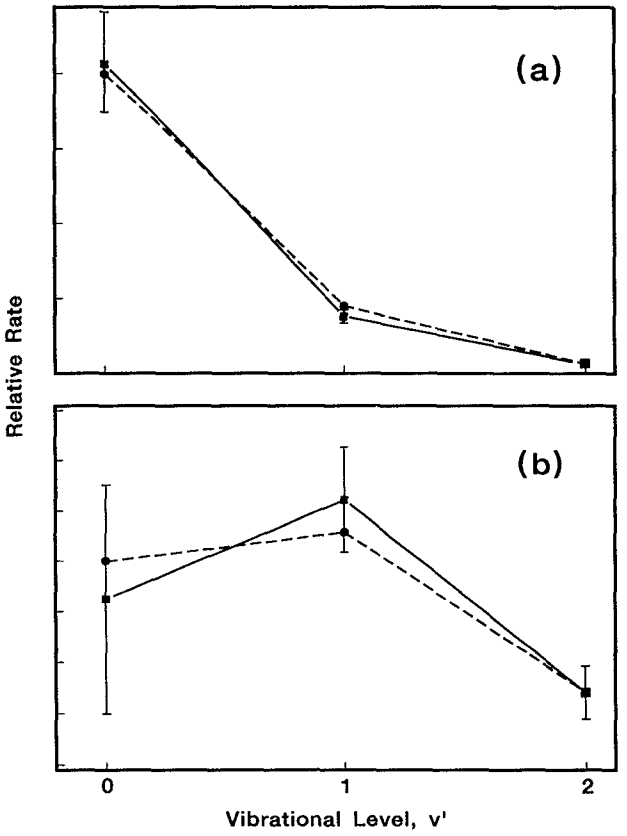

FIG. 18. Comparison of experimental (squares connected by solid lines) and quantum-mechanical (circles connected by dashed lines) vibrational population distributions of the HD product for (a) the $D+H_2(v=0,j)$ reaction and (b) the $D+H_2(v=1, j=1)$ reaction. Error bars represent one standard deviation.

Considerable time was spent exploring possible sources of experimental error, as described in this and the previous paper.[13] The checks for HD product fly-out (Sec. II B) and the new ILP experimental geometry were significant extensions of the previous experimental tests. While we would welcome independent confirmation of our results, we believe that it is unlikely that experimental errors persist of the magnitude needed to bring theory and experiment into accord. In addition, the theoretical calculations of NJK fully simulate the experimental initial conditions; therefore, although the discrepancies between experiment and theory are small we regard the existence of these deviations to be significant.

Two possibilities present themselves as the source of the remaining differences between experiment and theory. The first possibility is the accuracy of the H_3 potential energy surface. At higher energies the reactants can explore regions of the PES far removed from the minimum energy path of the reaction. These regions are less well characterized because *ab initio* points used to generate the surface are concentrated around the minimum energy path. The second possibility is nonadiabatic effects,[50,51] brought about by the presence of the avoided conical intersection between the ground and first excited state of the H_2D surface. Only additional theoretical work will be able to determine whether one or both of these possibilities account for the remaining discrepancies, assuming that the present experimental results are free from systematic error.

V. CONCLUSIONS

We have measured rates into the $HD(v'=0,1,2;j')$ product states for the reactions $D+H_2(v=0,j$ thermal) and $D+H_2(v=1, j=1)$ at several values of E_{rel}. In addition, a new experimental geometry has been introduced that permits independent control of the reagent rovibrational state, E_{rel}, and the product state probed.

A marked enhancement is found in the partitioning of energy into the product internal modes upon vibrational excitation of the H_2 reagent. We find that a model in which internal energy of the reagents appears as internal energy of the products (i.e., internal energy is conserved) provides a qualitative description of the dynamics of the reaction $D+H_2(v=1, j=1)$.

We find generally excellent agreement between the experiments using the DI precursor and QM theory; however, some small differences persist between the measured and predicted rotational distributions. We suggest that these discrepancies may be attributed to inaccuracies in the H_3 PES and/or nonadiabatic effects.

ACKNOWLEDGMENTS

We thank D. Neuhauser, R. S. Judson, and D. J. Kouri for many useful discussions and for making available to us the results of their theoretical calculations prior to publication. We would also like to thank A. Kuppermann for critical discussions of this work. D. E. Adelman

gratefully acknowledges the Natural Sciences and Engineering Research Council of Canada for a postgraduate scholarship. D. A. V. Kliner gratefully acknowledges the National Science Foundation for a predoctoral fellowship. This project was supported by the National Science Foundation under Grant No. NSF CHE-89-21198.

[1] J. C. Polanyi, Acc. Chem. Res. **5**, 161 (1972).
[2] D. P. Gerrity and J. J. Valentini, J. Chem. Phys. **81**, 1298 (1984).
[3] R. Götting, V. Herrero, J. P. Toennies, and M. Vodegel, Chem. Phys. Lett. **137**, 524 (1987).
[4] S. A. Buntin, C. F. Giese, and W. R. Gentry, J. Chem. Phys. **87**, 1443 (1987).
[5] G. W. Johnston, B. Katz, K. Tsukiyama, and R. Bersohn, J. Chem. Phys. **91**, 5445 (1987).
[6] H. B. Levene, D. L. Phillips, J.-C. Nieh, D. P. Gerrity, and J. J. Valentini, Chem. Phys. Lett. **143**, 317 (1988).
[7] K.-D. Rinnen, D. A. V. Kliner, and R. N. Zare, J. Chem. Phys. **91**, 7514 (1989).
[8] S. A. Buntin, C. F. Giese, and W. R. Gentry, Chem. Phys. Lett. **168**, 513 (1990).
[9] D. A. V. Kliner and R. N. Zare, J. Chem. Phys. **92**, 2107 (1990).
[10] R. E. Continetti, B. A. Balko, and Y. T. Lee, J. Chem. Phys. **93**, 5719 (1990).
[11] H. Buchenau, J. P. Toennies, J. Arnold, and J. Wolfrum, Ber. Bunsenges. Phys. Chem. **94**, 1231 (1990).
[12] D. A. V. Kliner, D. E. Adelman, and R. N. Zare, J. Chem. Phys. **94**, 1069 (1991).
[13] D. A. V. Kliner, D. E. Adelman, and R. N. Zare, J. Chem. Phys. **95**, 1648 (1991).
[14] J. Z. H. Zhang and W. H. Miller, Chem. Phys. Lett. **153**, 465 (1988).
[15] M. Mladenovic, M. Zhao, D. G. Truhlar, D. W. Schwenke, Y. Sun, and D. J. Kouri, J. Phys. Chem. **92**, 7035 (1988).
[16] D. E. Manolopoulos and R. E. Wyatt, Chem. Phys. Lett. **159**, 123 (1989).
[17] J. M. Launay and M. Le Dourneuf, Chem. Phys. Lett. **163**, 178 (1989).
[18] J. Z. H. Zhang and W. H. Miller, J. Chem. Phys. **91**, 1528 (1989).
[19] S. L. Mielke, R. S. Friedman, D. G. Truhlar, and D. W. Schwenke, Chem. Phys. Lett. **188**, 359 (1992); N. C. Blais, M. Zhao, D. G. Truhlar, D. W. Schwenke, and D. J. Kouri, Chem. Phys. Lett. **166**, 11 (1990).
[20] W. H. Miller, Annu. Rev. Phys. Chem. **41**, 245 (1990).
[21] M. Zhao, D. G. Truhlar, D. W. Schwenke, and D. J. Kouri, J. Phys. Chem. **94**, 7074 (1990).
[22] M. D'Mello, D. E. Manolopoulos, and R. E. Wyatt, J. Chem. Phys. **94**, 5985 (1991).
[23] S. L. Mielke, D. G. Truhlar, and D. W. Schenke, J. Chem. Phys. **95**, 5930 (1991).
[24] D. Neuhauser, J. Chem. Phys. **95**, 4927 (1991).
[25] W. J. Keogh, A. I. Boothroyd, P. Martin, S. L. Mielke, D. G. Truhlar, and D. W. Schwenke, Chem. Phys. Lett. **195**, 144 (1992).
[26] D. Neuhauser, R. S. Judson, and D. J. Kouri (unpublished).
[27] D. Neuhauser, R. S. Judson, D. J. Kouri, D. E. Adelman, N. E. Shafer, D. A. V. Kliner, and R. N. Zare, Science **257**, 519 (1992).
[28] D. A. V. Kliner, K.-D. Rinnen, and R. N. Zare, Chem. Phys. Lett. **166**, 107 (1990).
[29] J. C. W. Bauschlicher, S. R. Langhoff, and H. Partridge, Chem. Phys. Lett. **170**, 345 (1990).
[30] A. J. C. Varandas, F. B. Brown, C. A. Mead, D. G. Truhlar, and N. C. Blais, J. Chem. Phys. **86**, 6258 (1987).
[31] K.-D. Rinnen, D. A. V. Kliner, R. N. Zare, and W. M. Huo, Isr. J. Chem. **29**, 369 (1989); K.-D. Rinnen, M. A. Buntine, D. A. V. Kliner, R. N. Zare, and W. M. Huo, J. Chem. Phys. **95**, 214 (1991).
[32] K.-D. Rinnen, D. A. V. Kliner, R. S. Blake, and R. N. Zare, Rev. Sci. Instrum. **60**, 717 (1989).
[33] The BBO crystals were supplied by R. S. Feigelson and R. K. Route and grown as part of a research program sponsored in part by the Army Research Office, Contract No. DAAL03-86-K-0129, and in part by the NSF/MRL Program through the center for Materials Research, Stanford University.
[34] J. M. Khosrofian and B. A. Garetz, App. Opt. **22**, 3406 (1983).
[35] Y. R. Shen, *Principles of Nonlinear Optics* (Wiley-Interscience, New York, 1984).
[36] I. Levy and M. Shapiro, J. Chem. Phys. **89**, 2900 (1988).
[37] C. A. Taatjes and S. R. Leone (personal communication).
[38] R. Magnotta, D. J. Nesbitt, and S. R. Leone, J. Phys. Chem. **83**, 21 (1981).
[39] Z. Xu, B. Koplitz, and C. Wittig, Chem. Phys. Lett. **92**, 5518 (1988).
[40] A. E. Siegman, *Lasers* (University Science Books, Mill Valley, CA, 1986).
[41] P. M. Aker, G. J. Germann, and J. J. Valentini, J. Chem. Phys. **90**, 4795 (1989).
[42] P. M. Aker, G. J. Germann, K. D. Tabor, and J. J. Valentini, J. Chem. Phys. **90**, 4809 (1989).
[43] D. A. V. Kliner, K.-D. Rinnen, M. A. Buntine, D. E. Adelman, and R. N. Zare, J. Chem. Phys. **95**, 1663 (1991).
[44] R. Callaghan, Ph.D. thesis, University of Chicago, 1991.
[45] R. D. Levine and R. B. Bernstein, *Molecular Reaction Dynamics and Chemical Reactivity* (Oxford University Press, New York, 1980).
[46] I. Schechter, R. Kosloff, and R. D. Levine, Chem. Phys. Lett. **121**, 297 (1985).
[47] T. Drier and J. Wolfrum, Int. J. Chem. Kinet. **18**, 919 (1987).
[48] I. W. M. Smith, in *Advances in Gas-Phase Photochemistry and Kinetics*, edited by M. N. R. Ashford and J. E. Baggott (The Royal Society of Chemistry, London, 1989), p. 53.
[49] I. M. W. Smith, *Kinetics and Dynamics of Elementary Gas Reactions* (Butterworths, London, 1980).
[50] B. Lepetit and A. Kuppermann, Chem. Phys. Lett. **166**, 581 (1990).
[51] Y.-S. M. Wu, A. Kuppermann, and B. Lepetit, Chem. Phys. Lett. **186**, 319 (1991).